Copyrighted Materials
Copyright © 2002 Elsevier Retrieved from www.knovel.com

MACHINERY, ISOLATION

See **VIBRATION ISOLATION, APPLICATIONS AND CRITERIA**

MAGNETORHEOLOGICAL FLUIDS

See **ELECTRORHEOLOGICAL AND MAGNETORHEOLOGICAL FLUIDS**

MAGNETOSTRICTIVE MATERIALS

A Flatau, National Science Foundation, Arlington, VA, USA

Copyright © 2001 Academic Press

doi:10.1006/rwvb.2001.0079

The bidirectional coupling between the magnetic and mechanical states of a magnetostrictive material provides a transduction mechanism that is used in both sensing and actuation. The current interest in the design of adaptive smart structures, coupled with the advent of materials which exhibit high sensor figures of merit such as Metglas and the so-called giant magnetostrictive materials such as Terfenol-D has led to a renewed interest in the engineering of optimized magnetostrictive transducer designs. An overview of magnetostriction and of recent sensing and vibration control applications for magnetostrictive materials is presented along with a brief discussion of some pertinent magnetostrictive device design issues. Schematics of several actuator and sensor configurations are included, as are typical experimental results.

Magnetostriction and Magnetism

Magnetostrictive materials convert magnetic energy to mechanical energy and vice versa. As a magnetostrictive material is magnetized, it strains. Conversely, as either a force or torque produces a strain in a magnetostrictive material, the material's magnetic state changes. The application of either an external magnetic field or an external stress breaks the material's internal energy balance and leads to both magnetic responses (domain wall motion, magnetization rotation, and a change in permeability) and elastic responses (strain of the material and a change in stiffness).

Magnetostriction is an inherent material property associated with electron spin and orbit orientations and molecular lattice geometries and will not degrade with time or with use. The effect is not present when a magnetostrictive material is heated above its Curie temperature; however, the effect returns fully as the material is cooled to below the Curie temperature. All ferromagnetic materials exhibit magnetostriction; however, in many materials the magnitude of the strain or shape change is too small to be of consequence. Nominal longitudinal saturation strains for various materials at room temperature are shown in **Table 1**.

Sensors are commonly based on the reciprocal magnetostrictive effects, the change in magnetization and permeability of a sample that accompanies a change in an external stress or torque. The magnetization change produced due to the application of a stress is known as either the Villari effect or the magnetomechanical effect. The magnetization

change produced due to application of a torque is known as either the inverse Wiedemann effect or the Matteuci effect.

Actuators are commonly based on the shape change that accompanies magnetization of a magnetostrictive material. The most common shape change is a change in sample length, accompanied by a change in transverse dimensions. This is known as the Joule effect (after James Prescott Joule (1818–89) for positive identification of the change in length of an iron sample) or the magnetostrictive effect. Magnetostriction can also occur as a twisting which results from a helical magnetic field, often generated by passing a current through the magnetostrictive sample. This is known as the Wiedemann effect.

At low applied magnetic field strengths, domain wall motion occurs as a consequence of the growth of domains whose magnetization is aligned favorably with respect to the applied field, at the expense of domains with magnetization opposing the field. At moderate field strengths, the magnetic moments within unfavorably oriented domains overcome the anisotropy energy and suddenly rotate (jump) into one of the crystallographic easy axes closer to the external field direction. This jump coincides with a relatively large change in strain for a small change in applied field. At moderate to high field strengths, the magnetic moments align along crystallographically easy axes lying closest to the field direction. As the field is increased further, the magnetic moments undergo coherent rotation until they reach alignment with the applied field resulting in a single-domain material and technical saturation.

Crystalline growth can be tailored or optimized so as to enhance the magnetostrictive effect in a material of a given stoichiometry. For example, in the highly magnetostrictive alloy Terfenol-D ($Tb_xDy_{1-x}Fe_y$, where $x = 0.27-0.3$ and $y = 1.92-2.0$) energy minimization is satisfied with random alignment of the magnetic domain orientations along the eight outward diagonals from the center of the molecular cubic lattice such that the bulk sample has zero (or almost zero) net magnetization. Commercially available material is grown using directional solidification techniques and patented crystallographic growth methods that lead to crystal growth and magnetic moment orientations such that jumping of magnetization between easy axes perpendicular and parallel to the sample growth direction is facilitated.

Table 1 Saturation magnetostrictions for magnetostrictive materials at 300 °K

Material	*Magnetostriction* ($\Delta L/L \times 10^{-6}$)
Fe	−9
Ni	−35
Co	−60
60% Co–40%Fe	68
60% Ni–40%Fe	25
$TbFe_2$	1753
Terfenol-D	1600
$SmFe_2$	−1560
Metglas 2605SC	40

Data produced from Restorff JB (1994) *Encyclopedia of Applied Physics*, vol. 9, pp. 229–244.

Exchanges between magnetic and mechanical energy are the primary transduction effects employed in magnetostrictive sensing and actuation applications. The two coupled linear equations given in eqns [1] and [2] model these relationships. These equations neglect temperature effects and hysteresis, and have been reduced from a three-dimensional vector form to reflect only axial behavior. These magnetostrictive equations of state are expressed in terms of mechanical parameters (strain ε, stress σ, Young's modulus at constant applied magnetic field E^H), magnetic parameters (applied magnetic field H, magnetic induction B, permeability at constant stress μ^σ), and two piezomagnetic coefficients (these are also known as magnetomechanical coefficients and as axial strain coefficients: $d_{33} = \mathrm{d}\varepsilon/\mathrm{d}H|_\sigma$, and $d_{33}^* = \mathrm{d}B/\mathrm{d}\sigma|_H$, where for small strains, these two coefficients can be shown to be equal):

$$\varepsilon = \sigma/E_y^H + \mathrm{d}H \quad [1]$$

$$B = \mathrm{d}^*\sigma + \mu^\sigma H \quad [2]$$

where ε and B are dependent on the externally applied quantities σ and H. The elastic modulus, permeability, and piezomagnetic coefficients can vary significantly with operating conditions. They need to be experimentally determined and are usually provided by the material manufacturer. At present, most modeling codes rely on look-up tables to capture the time-varying and load-dependent nature of these coefficients.

These equations capture the low signal, linear, coupled mechanical, and magnetic nature of magnetostriction. Eqn [1] indicates that the net strain of a magnetostrictive element is the combined response to changes in stress (Hooke's law behavior, $\varepsilon = \sigma/E$) and applied magnetic field (Joule effect magnetostriction, λ). Eqn [2] indicates the simultaneous change in the magnetic induction of the element due to change in stress (reciprocal Joule or Villari effect magnetization) and applied field. This later effect can also be

expressed as a change in permeability by writing eqn [2] in a more general form:

$$B = \mu H \qquad [3]$$

In eqn [3] the effects of stress are included in the permeability, μ. Permeability can be monitored since both B and H can be related to measurable electrical quantities as described in eqns [4] and [5].

In the early nineteenth century, Oersted discovered that a moving charge generated a magnetic field in a plane perpendicular to the direction of charge motion. Thus, a current in a conductor could be used to produce a magnetic field around the conductor. Ampere's law describes this electromagnetic relationship. For a long, thin solenoid having a number of turns N_c and a length L_c a simple expression is derived;

$$H = (N_c I)/L_c \qquad [4]$$

Placing a magnetostrictive element inside such an excitation coil (solenoid) with an impressed current I provides an efficient means of magnetizing the element and producing controlled strain and force output.

The law of electromagnetic induction (Faraday–Lenz law) describes how a magnetic flux, $\varphi = BA_c$ in area A_c, induces a potential in an electrical conductor to which it is flux-linked. In its simplest differential form, the Faraday–Lenz law is given by:

$$V = -N_c \frac{\mathrm{d}\varphi}{\mathrm{d}t} = -N_c A_c \frac{\mathrm{d}B}{\mathrm{d}t} \qquad [5]$$

where V is the induced voltage in the solenoid of constant area A_c. According to this law, a potential will be induced in any electrically conducting material that makes up the magnetic circuit.

The excitation coil described by eqn [4] can be used to generate a magnetic field in a sample spatially separated from the coil. According to Gauss's law of magnetism:

$$\nabla \cdot B = 0 \qquad [6]$$

the divergence of B is zero. This means that the magnetic flux is always conserved. Thus magnetic flux lines close, defining a magnetic circuit, and elements of the magnetic circuit through which magnetic flux flows are said to be flux-linked. This makes it possible to magnetize one component of the magnetic circuit by generating a magnetic field in another component. Based on the principle expressed by eqns [5] and [6], it is possible to measure the magnetic flux density in a magnetic circuit by the voltage induced in a flux-linked detection coil.

Transduction

Magnetostrictive materials are magnetoelastic in the sense that they do work in the process of converting between magnetic and elastic (or mechanical) energy states. However, magnetostrictive transducers are generally classified as electromechanical devices or electromagnetomechanical because their input and output are generally electrical and mechanical in nature. The conversion of magnetic energy to and from electrical and/or mechanical is transparent to the device user. A common two-port schematic appropriate for both magnetostrictive sensing and actuation devices is given in **Figure 1**. The magnetostrictive driver is represented by the center block, with the transduction coefficients T_{me} (mechanical due to electrical) and T_{em} (electrical due to mechanical), indicative of both the magnetoelastic attributes characterized by eqns [1] and [2] and the electromagnetic attributes associated with conversion between electrical and magnetic fields characterized by eqns [4] and [5].

The transduction process relating the electrical and mechanical states can be described with two coupled linear equations. These canonical equations are expressed in terms of mechanical parameters (force F, velocity v, mechanical impedance Z_m), electrical parameters (applied voltage V, current I, electrical impedance Z_e), and the two transduction coefficients:

$$V = Z_e I + T_{em} v \qquad [7]$$

$$F = T_{me} I + z_m v \qquad [8]$$

Common magnetostrictive transducer components include a magnetic circuit, a solenoid for transduction of magnetic-to-electrical energy and vice versa, mechanisms for DC magnetic and mechanical (prestress) biasing. A generic magnetostrictive device con-

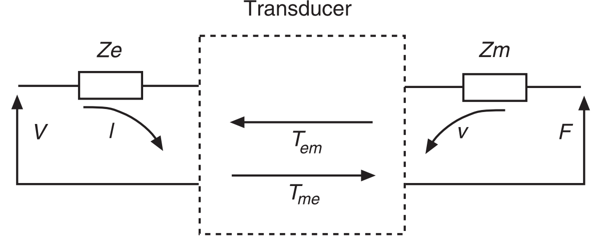

Figure 1 Two-port transducer schematic.

figuration is shown in **Figure 2**. The permanent magnet provides a DC magnetic field. The magnetic circuit passes though the magnetostrictive driver, end caps made of magnetic materials, and the permanent magnet. Belleville spring washers are used to provide an initial mechanical prestress. The solenoid can be used to provide both AC and DC magnetic fields for actuation purposes. Alternatively, for sensing applications, the change in voltage induced in the solenoid is to detect a change in strain and/or in the force applied to the device.

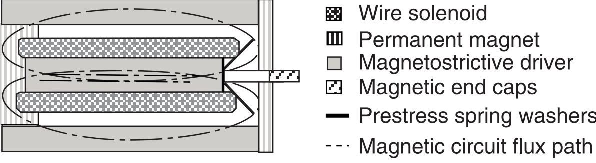

Figure 2 Components typical of a simple magnetostrictive transducer.

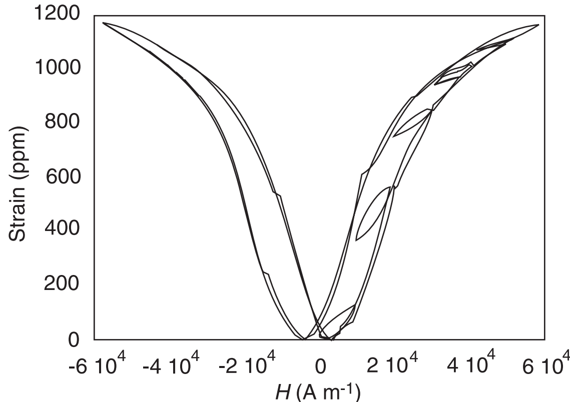

Figure 3 Strain vs applied-field major hysteresis loop and minor loops for AC fields of ± 5 kA m^{-1} at 0.7 Hz at DC bias levels of 5, 15, 25, 35, and 45 kA m^{-1}. Device mechanical load is a prestress of 6.9 MPa.

Figure 3 depicts a major hysteresis loop from an actuator similar in design to that shown in **Figure 2**. Superimposed on the major hysteresis loop are five minor hysteresis loops collected by driving at 0.7 Hz with an applied of ± 5 kA m^{-1} as the DC magnetic bias was increased from 5 to 45 kA m^{-1} in increments of 10 kA m^{-1}. AC operation of magnetostrictive actuators is typically achieved through the use of a DC magnetic field to provide bias operation so that it is centered about the steepest portion of the major hysteresis loop. This region is called the burst region, and the DC magnetic field amplitude required for operation about the middle of the burst region is called the critical field. All subsequent data are from magnetically biased transducers.

Figure 4 shows frequency response functions of acceleration per input current, where the change in the transducer's axial resonant frequency varies from 1350 Hz to over 2000 Hz, reflecting the effect of DC bias on the elastic modulus. The reduction in elastic modulus below that at magnetic saturation is known as the delta E effect. Note that in **Figure 4** only the axial resonant frequency of the magnetostrictive driver shifts and that the structural resonance of the device housing at 3300 Hz is not affected by the changing DC field.

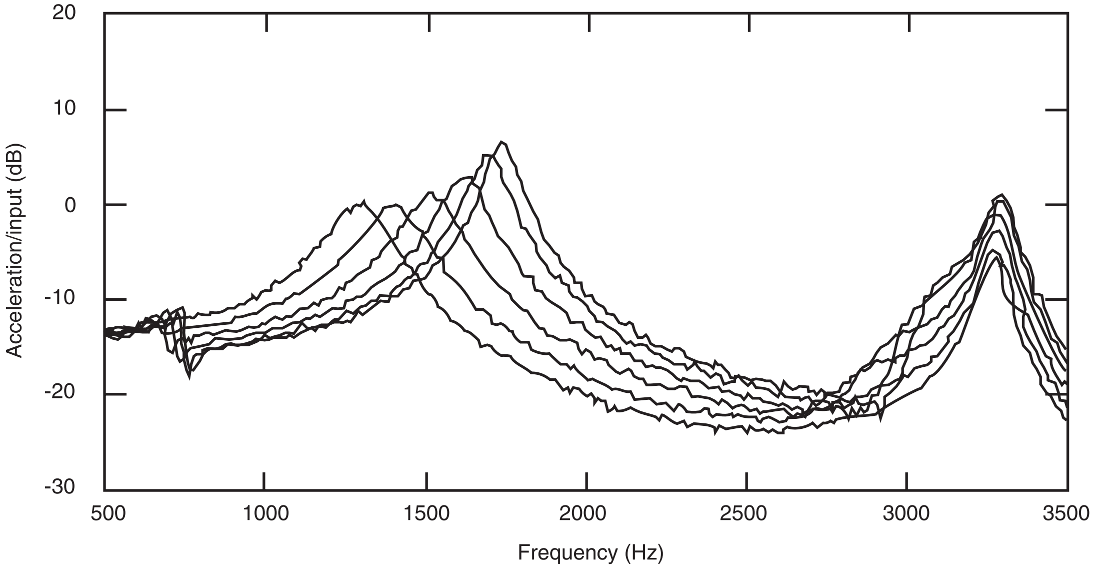

Figure 4 Acceleration per input current frequency response functions at DC bias levels of (from left to right): 20, 30, 36, 42, 50, and 60 kA m^{-1}.

Figure 5 illustrates the sensitivity of major strain-applied field hysteresis loops to variations in mechanical load or prestress. While this attribute allows tailoring of devices preloaded for optimized performance under a constant load (such as acoustic source applications), this introduces a parameter that must be optimized for operation under variable load conditions which are typical of vibration control applications. Actuators using tailored magnetostrictive composite drivers can minimize device sensitivity to variations in the external load.

The upper traces in **Figures 6–8** are Bode plots of strain per applied field, strain per magnetization and magnetization per applied field, respectively. The Bode plots were obtained using a swept sinusoidal signal at a relatively low signal excitation of the device (e.g., driving the device to produce maximum strains at resonance that are less than one-third of the device full strain potential, thereby minimizing the presence of undesired harmonics). The lower traces are minor hysteresis loops of these quantities recorded at (from left to right)

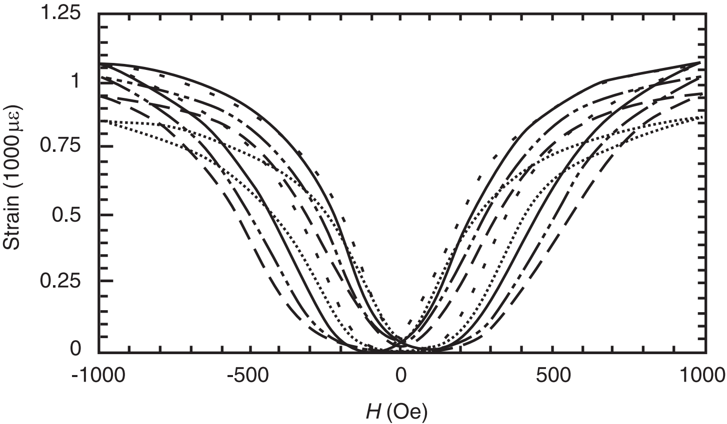

Figure 5 Strain vs applied-field major hysteresis loop corresponding to device mechanical loads of prestress: 3.5, 5.2, 6.9, 8.6 and 10.4 MPa. (–––) 1.5 ksi; (––––) 1.25 ksi; (—) 1.0 ksi; (-----) 0.75 ksi; (......) 0.5 ksi.

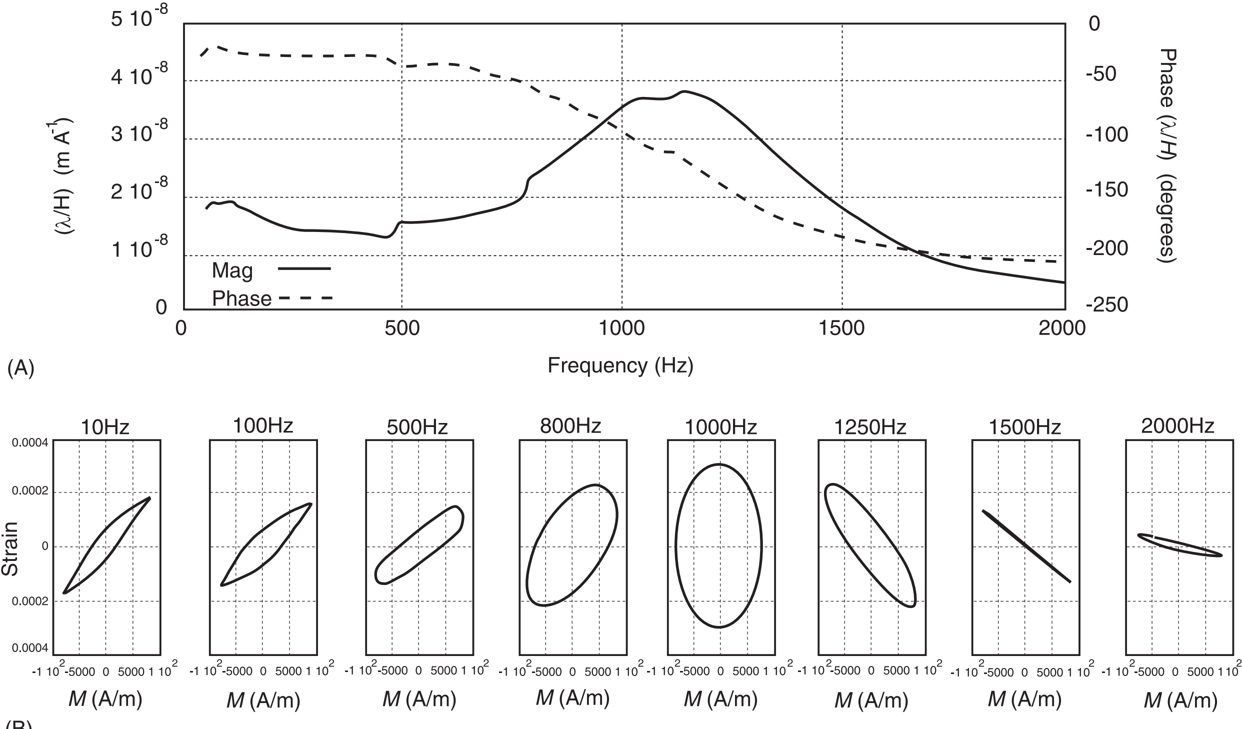

Figure 6 (A) Strain per applied magnetic field Bode plot. (B) Strain vs applied magnetic field minor loops ($\pm$400 microstrain vs $\pm$10 kA m^{-1}). From left to right, hysteresis minor loop data collected at: 10, 100, 500, 800, 1000, 1250, 1500, and 2000 Hz.

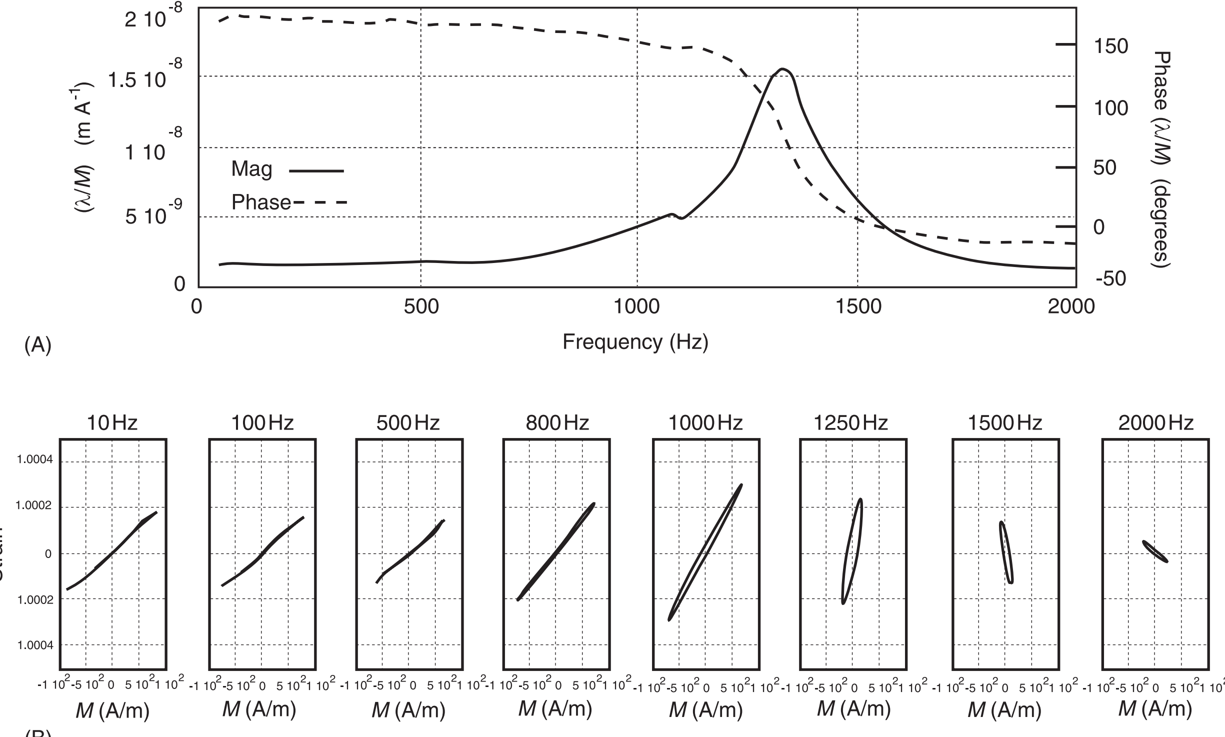

Figure 7 (A) Strain per magnetization Bode plot. (B) Strain vs magnetization minor loops ($\pm 100\,\mathrm{kA\,m^{-1}}$ vs $\pm 10\,\mathrm{kA\,m^{-1}}$). From left to right, hysteresis minor loop data collected at: 10, 100, 500, 800, 1000, 1250, 1500, and 2000 Hz.

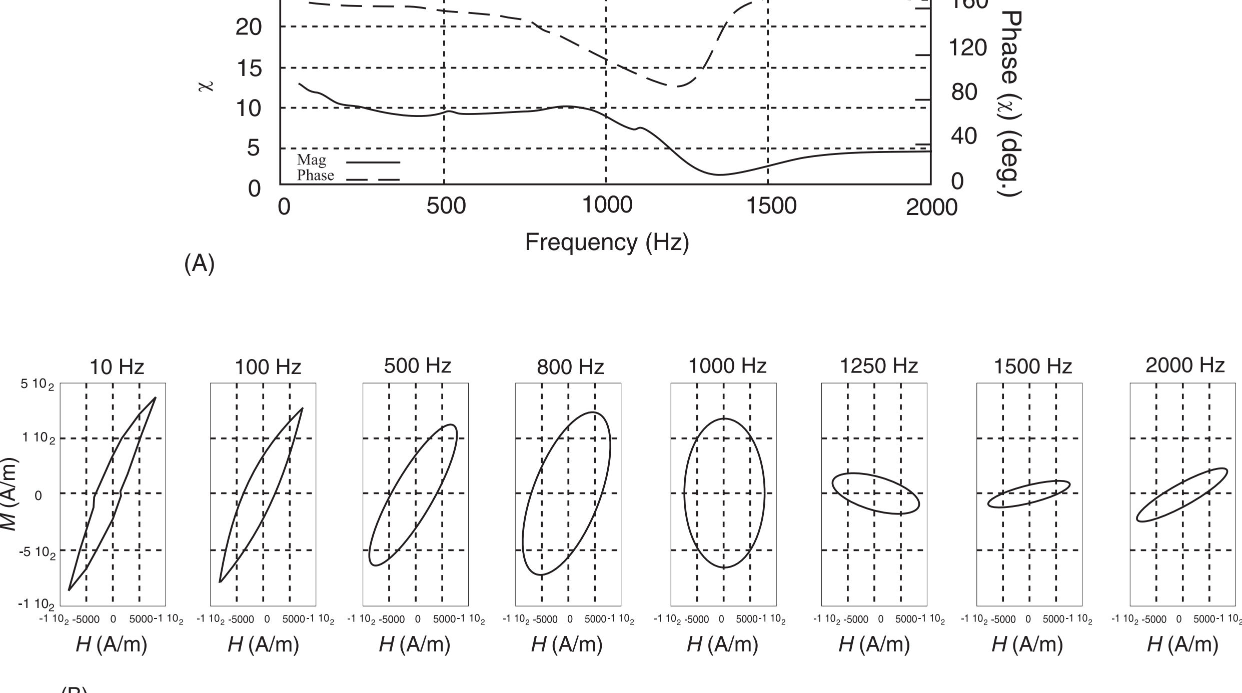

Figure 8 (A) Susceptibility (magnetization per applied field) Bode plot. (B) Susceptibility or magnetization vs applied-field minor loops (± 400 microstrain vs $\pm 100\,\mathrm{kA\,m^{-1}}$). From left to right, hysteresis minor loop data collected at: 10, 100, 500, 800, 1000, 1250, 1500, and 2000 Hz.

frequencies of 10, 100, 500, 800, 1000, 1250, 1500, and 2000 Hz.

Information on performance is used to implement calibration, input and/or output linearization, and control schemes to facilitate the optimized use of magnetostrictive devices. For example, information from **Figures 3** and **5** might be coupled to optimize the DC magnetic bias in real time to produce specified strains under varying mechanical loads. **Figure 4** demonstrates the ability to tune a system's resonant frequency in real time, which is the basis for a patent pending, tunable magnetostrictive vibration absorber design. This can be coupled with information on frequencies that minimize losses by using hysteresis loop data from **Figures 6–8** to tailor the frequency operation for the most efficient electromechanical performance. Additionally, this suggests the ability to target operating conditions for minimization of internal heating under continuous operation, which is of particular concern for ultrasonic operation.

Another significant loss factor that is associated with the transduction of electric to magnetic energy under dynamic operation is eddy currents. Eddy current power losses increase with approximately the square of frequency and thus have a significant impact on the operational bandwidth of devices. Laminations in the magnetostrictive core help to mitigate the effects of eddy currents, however, materials such as Terfenol-D are brittle and costly to laminate. Materials such as insulated magnetic particles or the silicon steels in common use in motors and power systems are suitable for the magnetic circuit components that make up the transducer housing, as they simultaneously support flux conduction and offer high resistivities. Magnetostrictive composites that use nonelectrically conducting matrix material yield reductions in eddy current losses. They have been proposed for extending device output bandwidth by an order of magnitude, from roughly 10 kHz to close to 100 kHz. Such composites offer great promise as high-frequency magnetostrictive drivers.

Actuation Configurations

Nickel was used in many of the early magnetostrictive sonar devices and is still being used in commercially available ultrasonic cleaners available from, for example, Blue Wave Ultrasonics. Other examples of magnetostrictive material use in commercial applications include Terfenol-D-based devices such as the underwater communication systems produced by Trigger Scuba, Inc., the acoustic pressure wave source (P-wave) produced by ETREMA Products, Inc. for enhancing oil well production rates, and precision micropositioners produced by Energenic, Inc.

Dynamic strains are of primary importance in low-frequency high-power transducers, namely those for sonar and underwater communications. At and near mechanical resonance, strains greater than the static saturation strain can be obtained. Three of the more common devices for sonar applications are the flextensional, the piston, and the 'ring' types of actuators. Flextensional transducers radiate acoustic energy through flexing of a shell, usually oval-shaped, caused by the longitudinal extension and contraction of a cylindrical drive motor mounted in compression inside the shell. The Tonpilz (Tonpilz is German for 'sound mushroom') transducer is a common piston-type design. The transducer has a magnetostrictive rod surrounded by a drive coil that provides AC and DC magnetic field excitation, a mechanism for pre-stressing the rod, a front radiating surface (piston), and a countermass. An advantage of piston-type designs over conventional flextensional transducers is that they lack parts likely to suffer fatigue-induced failure due to bending. A typical ring transducer might consist of four magnetostrictive rods that are arranged to form a square with four curved pistons that are the radiating surfaces enclosing the square and attached to the corners of the square. Monopole operation is achieved with the rods acting in unison. Dipole operation is accomplished by switching the magnetic bias on two of the rods and maintaining a constant direction on the AC magnetic field on all four rods. The interest in ring transducers during those early days was based on their ruggedness and lower cost compared to other available transducer technologies.

There is a growing interest in use of magnetostrictive devices as a source for motion and/or force, and in particular for use in conjunction with smart structures for active vibration control. These linear motor systems fall into the two general categories of piston devices and inchworm devices. An example of the performance that can be realized using magnetostrictive actuators for active vibration control is presented in **Figure 9** in which a simple analog proportion control scheme was applied to achieve significant vibration control (>33 dB at both mode 1 and 2). There are several variations on the inchworm motor concepts that move a shaft relative to the motor housing, and they all generally rely on two separate capabilities, a clamping force and a pushing force. Motors with linear shaft output rates of 20 mm s^{-1} have been designed that can develop 1000 N of force with a 200 mm stroke.

Although generic ultrasonic devices are similar to their low-frequency counterparts, e.g., they require the same components described in **Figure 2**, there are several problems associated with operation at

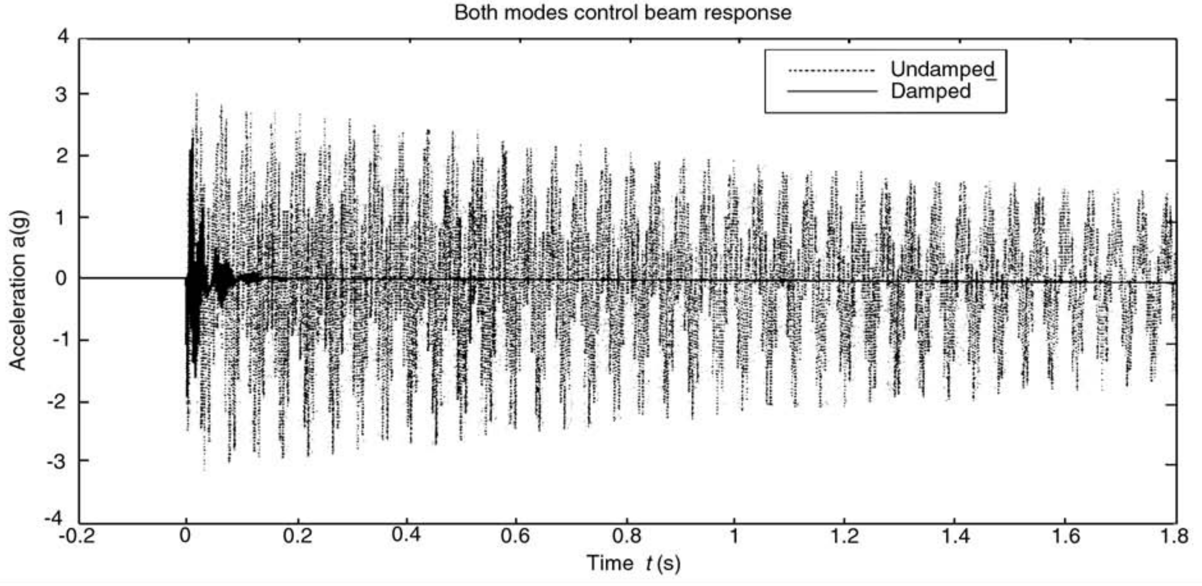

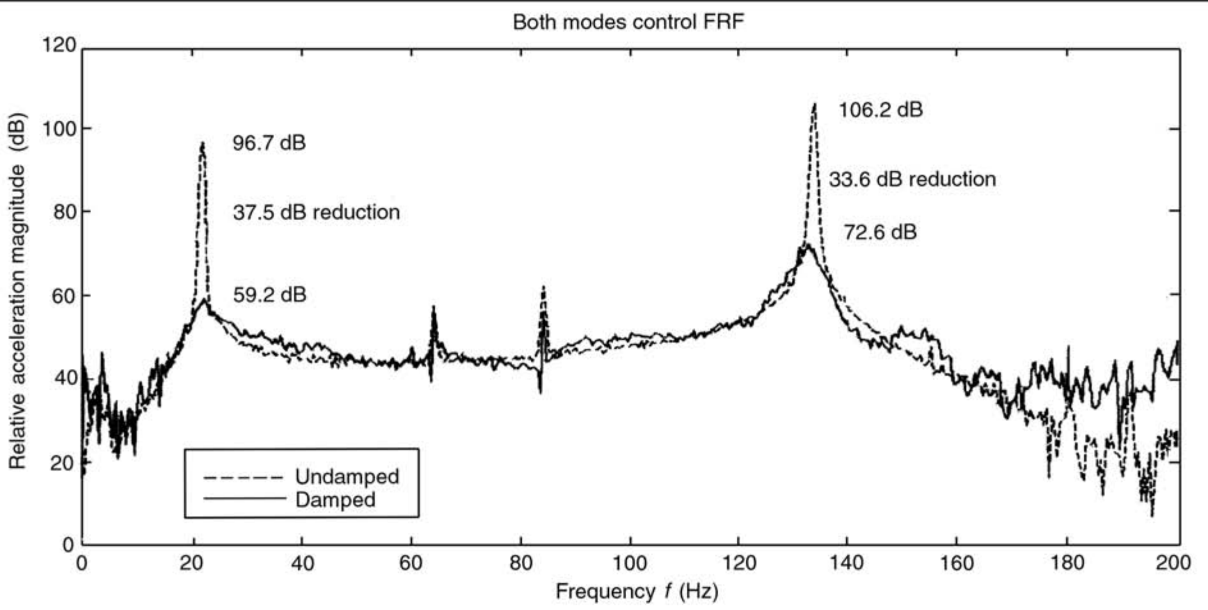

Figure 9 Magnetostrictive actuator performance for active vibration control of the transient responses of a 40 × 2 × 1 0.125-thick aluminum 'C' channel beam to impact excitation.

frequencies above 20 kHz. Hysteresis losses within a magnetostrictive driver will introduce high internal heat dissipation. Eddy currents will introduce both heat and a skin effect that effectively shields the core of the driver from an applied magnetic field. Impedance mismatches at ultrasonic frequencies make transfer of energy from the driver to the surrounding medium difficult. The use of laminated and/or composite magnetostrictive materials reduces losses associated with eddy currents. Device operation at resonance for enhanced energy output is often obtained through the use of quarter-wavelength-long drivers in conjunction with half-wavelength amplifying horns having application specific profiles.

Sensing Configurations

Magnetostrictive sensors can be classified as passive sensors, active sensors, and combined or hybrid sensors, based on how the magnetomechanical properties of the system components are used to measure the parameters of interest.

Passive sensors rely on magnetomechanical coupling to link a measurable change in the magnetostrictive material to the external property or condition of interest. For example, according to the Villari effect, the change in the magnetization of the magnetostrictive sample is correlated to an externally imposed change in stress. A coil flux-linked to the magnetostrictive sample can be used to measure changes in magnetic flux as per eqn [5]. Quantities such as external load, force, pressure, vibration, and flow rates can then be measured.

Active sensors use an internal excitation of the magnetostrictive element to facilitate some measurement of the magnetostrictive element that changes with the external property of interest. For example, an excitation coil could be used to excite the magnetostrictive sample with a known H as per eqn [4] and the detection coil used to measure B as per eqn [5]. The permeability from eqn [3] can then be monitored for changes due to an external condition. Designs that employ two coils, one to excite the magnetostrictive element and one for measurement, are known as transformer-type sensors. The most common active sensor design mentioned in the literature is the noncontact torque sensor. Many configurations employ variations on a general theme of a magnetostrictive wire, thin film, or ribbon flux-linked to a target shaft subject to a torque. The change in the magnetic induction or permeability can then be related to the torque on the specimen.

Finally, combined or hybrid sensors use a magnetostrictive element actively to excite or change another material to allow measurement of the property of interest. For example, a fiberoptic magnetic field sensor uses the change in length of a magnetostrictive element in the presence of a magnetic field (Joule effect) to change the optical path length of a fiberoptic sensor. Stress can be measured using photoelastic material, and highly accurate displacement measurements can be made with the help of a magnetostrictive guide.

Magnetostrictive transducers are particularly attractive for noncontact torque and position sensor applications. As a magnetostrictive shaft is torqued, stress develops at $\pm 45^{\circ}$ from the shaft axis, and the Villari effect produces changes in the shaft magnetization and permeability. The change in magnetization can be measured directly with a Hall probe. Alternatively, the change in permeability can be measured using a two-solenoid active technique in which an excitation solenoid is used to apply a constant magnetic field to a magnetic circuit flux-linked to the shaft and a detection solenoid monitors the torque-induced changes in the magnetic circuit permeability. These torque-induced changes can also be monitored by tracking electrical impedance function changes in flux-linked excitation and/or detection solenoids, as suggested by the data in **Figure 10**.

Several approaches exist for extending this technology to nonferromagnetic materials, by applying magnetostrictive materials directly to the surface of the rotating shafts. One technique relies on using amorphous magnetostrictive wire or ribbons that are helically wrapped around and bonded to a shaft. In another, at a high temperature the wire is exploded into fine particles which adhere strongly to the shaft.

Similarly, noncontact position sensors and force distribution sensors are available that respond to the influence of reflected signals and gaps on magnetostrictive components of a magnetic circuit (magnetostrictive waveguides and magnetostrictive delay lines, respectively). Metglas amorphous ribbons are an attractive strain sensor material because they exhibit large permeability changes in response to strain.

Velocity and force can be directly measured in a magnetostrictive transducer, as depicted in **Figure 2**, where the voltage induced in the solenoid is proportional to the velocity of the force applied to the free end of the magnetostrictive element. Similar transducers have been used as colocated sensor–actuator devices; e.g., devices that simultaneously actuate and sense. The telephone, scanning sonar, and active vibration control applications have made use of this dual operation mode. Although this can be accomplished by separating the voltage induced in the excitation solenoid via the Faraday–Lenz law from the applied (excitation) voltage, the sensed voltages is generally much smaller than that needed for actuation. Hence, it is common for a dual-mode transducer to use separate excitation and detection solenoids.

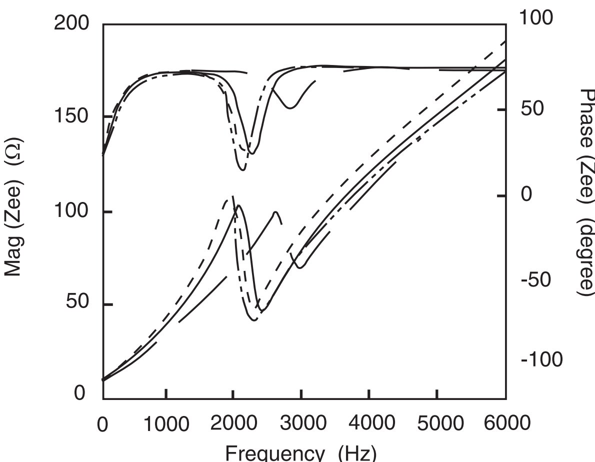

Figure 10 Sensitivity of electrical impedance functions to changes in the stress in the transducer magnetostrictive element. (Key as in **Figure 5**.)

Nomenclature

A	area
B	magnetic induction
F	force
H	magnetic field
T	current
L	length
N	number of terms
T	transduction
v	velocity
V	applied voltage
Z	impedance
ε	strain
λ	Joule effect magnetostriction
σ	stress

See also: **Actuators and smart structures**; **Electrorheological and Magnetorheological Fluids**; **Sensors and actuators**; **Transducers for absolute motion**; **Transducers for relative motion**.

Further Reading

Butler JL (1988) *Application Manual for the Design Etrema Terfenol-D. Magnetostrictive Transducers*. Ames, IA: Edge Technologies.

Calkins FT (1997) PhD dissertation, Iowa State University.

Cedell T (1995) *Magnetostrictive Materials and Selected Applications*. PhD dissertation, Lund University, Sweden.

Clark A (1980) *Magnetostrictive Rare Earth-Fe_2 Compounds, Ferromagnetic Materials*, vol.1. Amsterdam: North-Holland.

Cullity BD (1972) *Introduction to Magnetic Materials*. Reading, MA: Addison Wesley.

Dapino MJ, Calkins FT and Flatau AB (1999). In Webster JG (ed.) *Wiley Encyclopedia of Electrical and Electronics Engineering*, vol. 12, pp. 278–305. Chichester, UK: Wiley.

du Tremolet de Lacheisserie E (1993) *Magnetostriction Theory and Applications of Magnetoelasticity*. Boca Raton: CRC Press.

Fleming W (1990) Magnetostrictive torque sensors – comparison of branch, cross, and solenoidal designs. SAE Technical Paper 900264, pp. 51–78.

Hunt FV (1982) *Electroacoustics: The Analysis of Transduction, and its Historical Background*. American Institute of Physics for the Acoustical Society of America.

Jiles D (1991) *Introduction to Magnetism and Magnetic Materials*. London: Chapman and Hall.

NDRC (1946) Summary of Technical Report of Division 6. The design and construction of magnetostriction transducers, Vol. 13.

Restorff JB (1994) *Encyclopedia of Applied Physics*, vol. 9, pp. 229–244.

MATERIALS, DAMPING

See **DAMPING MATERIALS, SEISMIC INSTRUMENTS, ENVIRONMENTAL FACTORS, LASER BASED MEASUREMENTS**

MEASUREMENT

See **LASER BASED MEASUREMENTS; SEISMIC INSTRUMENTS, ENVIRONMENTAL FACTORS; STANDARDS FOR VIBRATIONS OF MACHINES AND MEASUREMENT PROCEDURES; TRANSDUCERS FOR ABSOLUTE MOTION; TRANSDUCERS FOR RELATIVE MOTION**

MEMBRANES

A W Leissa, Ohio State University, Columbus, OH, USA

Copyright © 2001 Academic Press

doi:10.1006/rwvb.2001.0132

A membrane is a structural element which is very thin in one direction compared with the other two, and is flat. In contrast with a plate, it has no bending or twisting stiffness. If a membrane is not flat, it is called a 'membrane shell' (see **Shells**). The membrane is stretched in its plane by tensile and (perhaps) shear stresses. It is these stresses which provide the restoring forces during transverse free vibrations. It is also assumed that these stresses are sufficiently large so that, if the transverse vibrational displacement (w) is kept small, the stresses will remain constant during

vibration. **Figure 1** depicts a membrane in its static equilibrium position, stretched over a boundary of arbitrary curvilinear shape. The stress (force/area) applied externally is shown as a normal stress σ_n which may vary along the boundary. In addition, a variable shear stress, which is not shown, may also act in the plane (xy) of the membrane, and tangent to its boundary. These boundary stresses cause internal normal stresses (σ_x and σ_y) and shear stress (τ_{xy}), as shown on an internal element of the membrane in **Figure 1**, which may vary with the coordinates (x and y), but not with time (t).

The equation of transverse motion of the membrane is:

$$T_x \frac{\partial^2 w}{\partial x^2} + 2T_{xy}\frac{\partial^2 w}{\partial x\,\partial y} + T_y\frac{\partial^2 w}{\partial y^2} + q = \rho h \frac{\partial^2 w}{\partial t^2} \quad [1]$$

where T_x, T_{xy}, T_y are the stress resultants (force/length) obtained by multiplying σ_x, τ_{xy} and σ_y, respectively, by the thickness (h). Transverse forcing pressure (force/area) is indicated by q, which could be present in a forced vibration situation, and ρ is the mass density/volume. In eqn [1], T_x, T_{xy}, T_y, ρ and h may each be functions of x and y, but not t.

Considering free, undamped vibrations ($q = 0$), the most widely used form of eqn [1] is the special case wherein the in-plane shear stress is zero, and the remaining tensile stress is constant and the same in all directions ($T_x = T_y = T$). In this case eqn [1] becomes:

$$T\nabla^2 w = \rho h \frac{\partial^2 w}{\partial t^2} \quad [2]$$

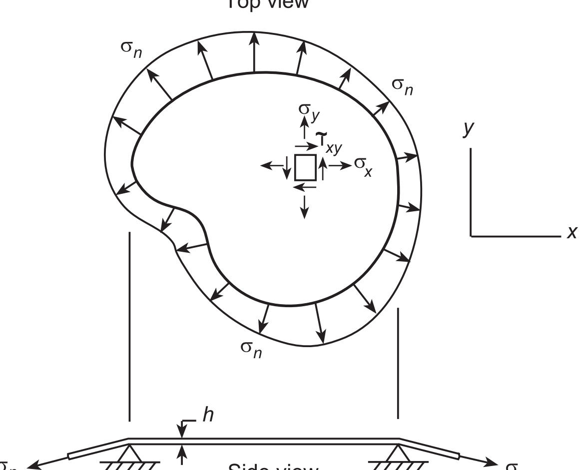

Figure 1 Membrane of arbitrary shape subjected to nonuniform tensile stress.

where $\nabla^2 = \partial^2/\partial x^2 + \partial^2/\partial y^2$ is the Laplacian differential operator.

Rectangular Membranes

Consider first a rectangular membrane with dimensions $a \times b$, stretched by uniform tension (T). Let the origin of the xy coordinate system be in one corner, so that the four edges ($x = 0, a; y = 0, b$) are fixed ($w = 0$). An exact solution for the transverse, free vibration displacement is:

$$w(x, y, t) = \sin(m\pi x/a)\sin(n\pi y/b)\sin(\omega t + \phi) \quad [3]$$

where m and n are integers, ranging from one to infinity ($m, n = 1, 2 \ldots \infty$), and ϕ is an arbitrary phase angle. It is seen that eqn [3] satisfies the boundary condition ($w = 0$) along all four edges. Substituting it into eqn [2] yields the natural frequencies (ω), which are conveniently expressed in terms of the nondimensional parameter:

$$\omega a\sqrt{\rho h/T} = \pi\left[m^2 + (a/b)^2 n^2\right]^{1/2} \quad [4]$$

Looking at eqn [4] it is clear that the fundamental (i.e., lowest) frequency of a rectangular membrane, regardless of the aspect ratio (a/b) will be for a mode shape having one half-sine wave in each direction ($m = n = 1$). **Figure 2** shows the first nine nodal patterns of free vibration for a rectangular membrane having $a/b = 1.5$. The dashed lines are node lines ($w = 0$). The corresponding nondimensional frequencies $\omega a\sqrt{\rho h/T}$ are 5.664, 7.854, 9.935, 10.538, 11.327, 13.329, 13.421, 14.482, and 15.471, according to eqn [4]. It is seen that some frequencies may be quite close together.

One may also have two mode shapes having the same frequency. These are called 'degenerate modes'. For example, consider the square membrane ($a = b$) and its degenerate frequencies $\omega_{12} = \omega_{21}$. Because they both vibrate with the same frequency, superposition of the two mode shapes may be taken as:

$$W(x, y) = C_{12}\sin(\pi x/a)\sin(2\pi y/a) + C_{21}\sin(2\pi x/a)\sin(\pi y/a) \quad [5]$$

where C_{12} and C_{21} are arbitrary constants, determined by how the membrane is set into motion (the initial conditions). **Figure 3** shows how the node line varies with the relative magnitude (C_2/C_1) of the superimposed modes. **Figure 3** also shows some

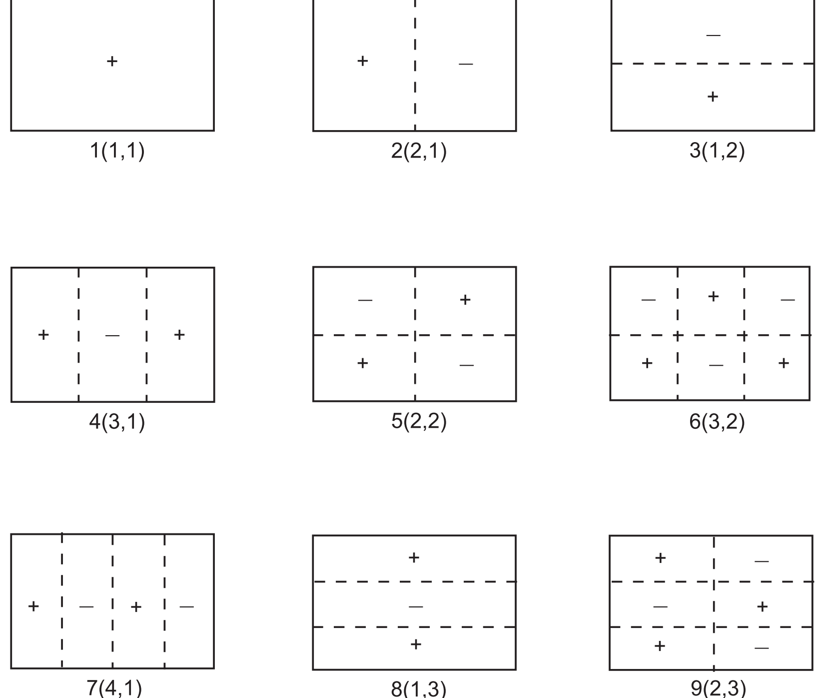

Figure 2 First nine nodal patterns of a rectangular membrane with $a/b = 1.5$.

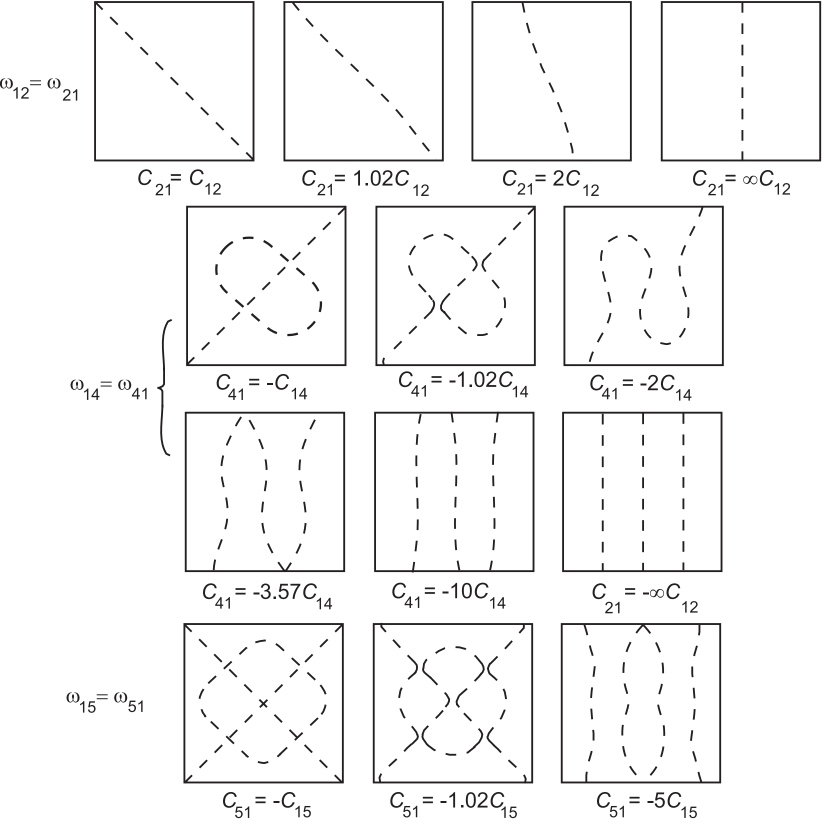

Figure 3 Some superimposed degenerate nodal patterns for square membranes.

superimposed degenerate modes for $\omega_{14} = \omega_{41}$, and for $\omega_{15} = \omega_{51}$.

Circular Membranes

For a circular membrane it is convenient to use polar coordinates, as shown in **Figure 4**. Then $\nabla^2 = \partial^2/\partial r^2 + (1/r)\partial/\partial r + (1/r^2)\partial^2/\partial\theta^2$. By separation of variables one finds the transverse displacement:

$$w(r, \theta, t) = [A_n J_n(kr) + B_n Y_n(kr)] \cos\ n\theta \sin(\omega t + \phi) \qquad [6]$$

which satisfies eqn [2] exactly, where J_n and Y_n are Bessel functions of the first and second kinds, respectively, $k^2 = \omega^2 \rho h/T$, A_n and B_n are arbitrary constants, and n is an integer, beginning with zero. Because $Y_n(0) = -\infty$, it is necessary to set $B_n = 0$ to have finite displacement at the center $(r = 0)$. Setting $w = 0$ along the boundary $(r = a)$ results in the frequency equation:

$$J_n(ka) = 0 \qquad [7]$$

The first five roots $ka = \omega a\sqrt{\rho h/T}$ of eqn [7] are given in **Table 1** for each n. Nodal patterns for the first nine frequencies of a circular membrane are shown in **Figure 5**, along with the corresponding $\omega a\sqrt{(\rho h/T)}$ It is seen that modes 1, 4, and 9 are axisymmetric $(n = 0)$, having 0, 1, and 2 interior nodal circles, respectively, whereas modes 2, 3, 5, and 7 have 1, 2, 3, and 4 nodal diameters, respectively, with no interior nodal circles. Exact shapes of the vibration modes along diameters may be seen from plots of the Bessel functions $J_n(kr)$.

An annular membrane is bounded by two concentric circles, an inner one at $r = b$, and an outer one at $r = a$, with both circular boundaries being fixed and exerting uniform radial tension T (force/length). The solution (eqn [6]) of eqn [3] is again

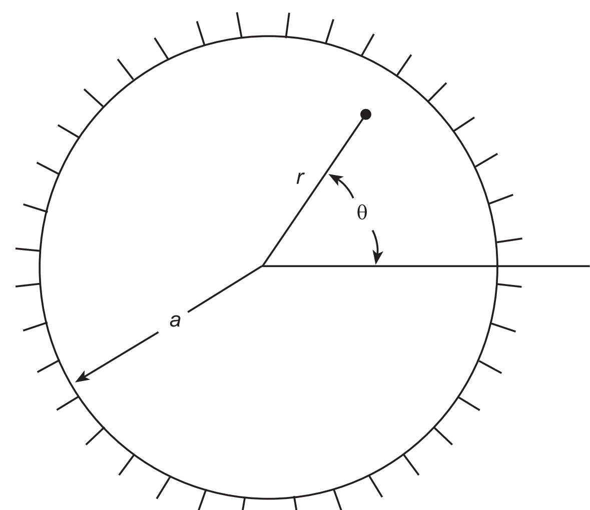

Figure 4 Circular membrane and polar coordinates.

appropriate. But both A_n and B_n are now retained, because $r = 0$ does not apply to the membrane. Setting $w = 0$ at $r = a$ and $r = b$ gives, for a nontrivial solution, the following frequency equation:

$$J_n(\lambda) Y_n\left(\frac{b}{a}\lambda\right) - J_n\left(\frac{b}{a}\lambda\right) Y_n(\lambda) = 0 \qquad [8]$$

where $\lambda = ka = \omega a\sqrt{\rho h/T}$. For any desired value of b/a, all frequencies of the annular membrane are obtainable from eqn [8]. The first three frequencies (corresponding to 0, 1, and 2 interior nodal circles) are listed in **Table 2** for the $n = 0$ (axisymmetric) and $n = 1$ (one nodal diameter) modes of annular membranes having various b/a ratios, especially for $b/a < 0.5$. It is interesting to note that, as b/a approaches zero, which corresponds to a central point support, the frequency for $n = 0$ becomes the same as for the unsupported membrane (**Table 1**). This is because membranes are incapable of transmitting transversely applied concentrated forces (reactive in this situation)

Table 1 Frequencies $\omega a\sqrt{\rho h/T}$ for circular membranes.

	n (nodal diameters)					
Number of root[a]	*0*	*1*	*2*	*3*	*4*	*5*
1	2.405	3.832	5.136	6.380	7.588	8.771
2	5.520	7.016	8.417	9.761	11.065	12.339
3	8.654	10.173	11.620	13.015	14.373	15.700
4	11.792	13.324	14.796	16.223	17.616	18.980
5	14.931	16.471	17.960	19.409	20.827	22.218

[a] Number of nodal circles plus one.

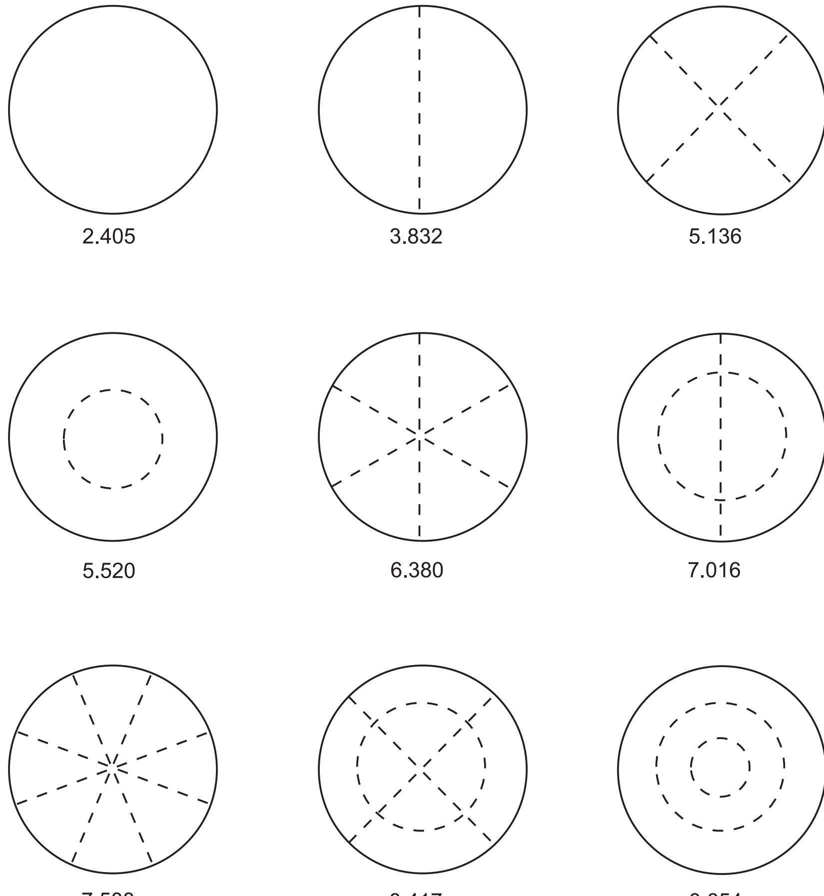

Figure 5 First nine nodal patterns of a circular membrane.

Table 2 Frequencies $\omega a\sqrt{\rho h/T}$ for annular membranes.

		Number of roots		
n	*b/a*	*1*	*2*	*3*
0	0.80	15.698	31.411	47.121
	0.60	7.828	15.695	23.553
	0.40	5.183	10.443	15.688
	0.20	3.816	7.786	11.732
	0.10	3.314	6.858	10.377
	0.02	2.884	6.136	9.376
	0.00	2.405	5.520	8.654
1	0.80	15.738	31.431	47.134
	0.60	7.930	15.747	23.588
	0.40	5.391	10.558	15.766
	0.20	4.236	8.055	11.927
	0.10	3.941	7.331	10.748
	0.02	3.836	7.031	10.205
	0.00	3.832	7.016	10.173

without violating the linearizing assumptions made in deriving the theory.

Other Shapes

A sectorial membrane has the shape of a sector of a circle (**Figure 6**), with a sector angle, α. The transverse displacement:

$$w(r,\theta,t) = [A_\upsilon J_\upsilon(kr) + B_\upsilon Y_\upsilon(kr)] \sin \upsilon\theta \sin(\omega t + \phi) \quad [9]$$

satisfies eqn [2]. Moreover, if noninteger values of υ are chosen such that $\upsilon = n\pi/\alpha (n = 1, 2 \ldots \infty)$, then $w = 0$ along the radial edges $\theta = 0$ and α, as desired. Setting B_υ=0 to avoid infinite displacement at $r = 0$, and $w = 0$ at $r = a$ yields:

$$J_\upsilon(ka) = 0 \quad [10]$$

Symmetric modes result from $n = 1, 3, \ldots$; antisymmetric modes from $n = 2, 4, \ldots$ For every υ there is an infinite number of nondimensional frequencies $ka = \omega a\sqrt{\rho h/T}$. Frequencies arising from half-integer orders of υ are given in **Table 3**. Results for intermediate values of $\alpha = 180^\circ, 90^\circ, 60^\circ, 45^\circ$, and 36°, corresponding to integer υ, may be taken from **Table 1**. The case of $\upsilon = 1/2$, corresponding to $\alpha = 360^\circ$ in **Table 3**, yields boundaries at $\theta = 0^\circ$ and $\theta = 360^\circ$, which are the same radial line, and the case of the complete circular membrane supported along an additional single radial line is thereby represented.

Annular sectorial membranes are bounded by the circle arcs $(r = b, r = a)$ and the two radial lines $(\theta = 0, \theta = \alpha)$. Frequencies for arbitrary α and b/a may be found from eqn [8], replacing n by υ, where $\upsilon = n\pi/\alpha (n = 1, 2 \ldots \infty)$.

Because node lines have the same zero transverse displacement as a constrained boundary, considerable miscellaneous results for other membrane shapes

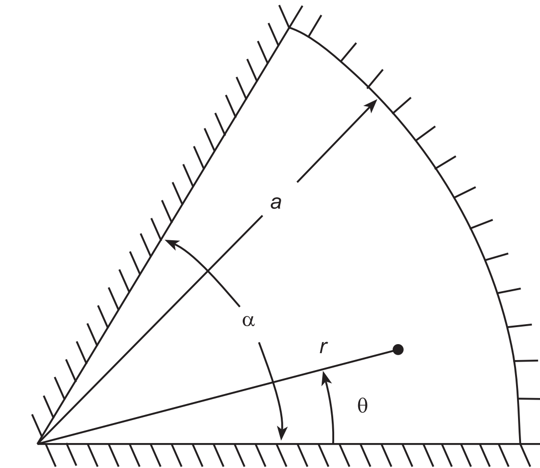

Figure 6 Sectorial membrane.

can be found by studying nodal patterns. For example **Figure 3** shows that the exact frequency for an isosceles right triangle with sides $a \times a$ is that of the (1, 2) and (2, 1) modes of a square $-\omega a\sqrt{\rho h/T} = \sqrt{5}\pi$. Considering the node lines as boundaries, **Figure 3** also shows a variety of shapes, each having straight and curvilinear lines as boundaries.

Additional information for straight-sided membranes may be obtained from published results for plates having the same configurations and all edges simply supported, using the correspondence:

$$\left(\frac{\omega_m^2 \rho h}{T}\right)^2 \sim \frac{\omega_p^2 \rho h}{D} \quad [11]$$

where the subscripts m and p correspond to membrane and plate natural frequencies, respectively (see **Plates**). Using this one can, for example, obtain the accurate frequencies for right triangular membranes of various aspect ratios (b/a) presented in **Table 4**. Corresponding nodal patterns for the second, third,

Table 3 Frequencies $\omega a\sqrt{\rho h/T}$ for sectorial membranes.

	Sector angle, α (and value of ν)					
Number of roots[a]	*360° (1/2)*	*120° (3/2)*	*72° (5/2)*	*51.43° (7/2)*	*40° (9/2)*	*32.73° (11/2)*
1	3.142	4.493	5.763	6.988	8.183	9.356
2	6.283	7.725	9.095	10.418	11.705	12.967
3	9.425	10.904	12.323	13.698	15.040	16.355

[a] Number of nodal circles plus one.

Table 4 Frequencies $\omega a\sqrt{\rho h/T}$ for right triangular membranes

	b/a					
Mode number	*1*	*1.25*	*1.5*	*2*	*2.5*	*3*
1	7.025	6.323	5.855	5.269	4.907	4.679
2	9.935	8.876	8.099	7.063	6.408	5.967
3	11.33	10.25	9.584	8.641	7.781	7.147
4	12.95	11.48	10.32	9.018	8.482	8.142

Adapted from more extensive data given in: Gorman DJ (1983) A highly accurate analytical solution for free vibration analysis of simply supported right triangular plates. *Journal of Sound and Vibration* 89: 107–118.

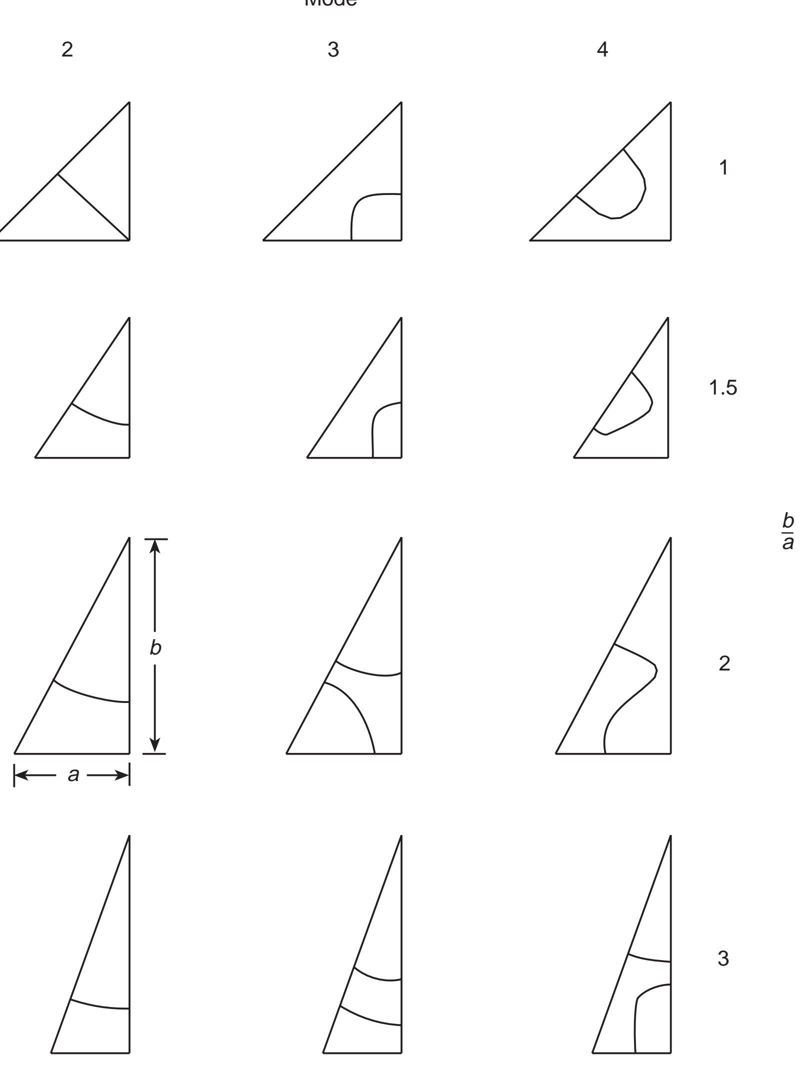

Figure 7 Nodal patterns for the second, third, and fourth modes of right triangular membranes.

Table 5 Nondimensional frequencies $\omega a\sqrt{\rho h/\sigma_x}$ for a square membrane with biaxial tension ($\sigma_y = \sigma_x$) and additional shear stress (τ_{xy})

	Mode number						
τ_{xy}/σ_x	*1*	*2*	*3*	*4*	*5*	*6*	*7*
0.00	4.443	7.025	7.025	8.886	9.935	9.935	11.327
0.10	4.438	6.916	7.118	8.837	9.922	9.962	11.092
0.20	4.425	6.790	7.197	8.701	9.886	10.030	10.801
0.50	4.322	6.285	7.337	7.934	9.603	9.606	10.606
0.75	4.126	5.620	6.864	7.306	8.099	9.062	9.268
0.85	3.986	5.211	6.221	7.212	7.221	8.149	8.678
0.98	3.591	4.174	4.647	5.110	5.584	6.114	6.802
1	3.376	3.677	4.015	4.411	4.889	5.488	6.280

Adapted from more extensive data given in: Leissa AW, Ghamat-Rezaei A (1990). Vibration of rectangular membranes subjected to shear and nonuniform tensile stresses. *Journal of the Acoustical Society of America* 88: 231–238.

and fourth modes are exhibited in **Figure 7**. (The first modes have no interior node lines.)

Some Complicating Effects

Results for frequencies and mode shapes of free vibrations given above have all been for membranes which are initially stretched by a uniform tensile stress resultant (T) in all directions. If a rectangular membrane is subjected to different, but uniform, tensile stresses in its lengthwise and breadthwise direction ($T_x = \sigma_x h =$ constant, $T_y = \sigma_y h =$ constant), the sine wave mode shapes of eqn [3] remain valid. Substituting eqn [3] into eqn [1], with $q = 0$ and $T_{xy} = 0$, yields the exact frequencies:

$$\omega a\sqrt{\rho h/T_x} = \pi\left[m^2 + (T_y/T_x)(a/b)^2 n^2\right]^{1/2} \quad [12]$$

If shear stress is also present then no exact solution is possible. Let σ_x, σ_y, and τ_{xy} all be constants. Reasonably accurate frequencies for a square membrane ($a/b = 1$), with $\sigma_y = \sigma_x$ and varying amounts of additional shear stress (τ_{xy}/σ_x), were obtained by the Ritz method, and are presented in **Table 5**. For this combination of stresses, the stresses along 45° diagonal planes are principal stresses:

$$\sigma_1 = \sigma_x + \tau_{xy}, \quad \sigma_2 = \sigma_x - \tau_{xy}, \quad \tau_{12} = 0 \quad [13]$$

as shown in **Figure 8**. As τ_{xy}/σ_x approaches unity, σ_2 becomes zero, and σ_1 becomes $2\sigma_x$. This is a special case of diagonal tension where the membrane is stretched in the direction of one of its diagonals, but is slack in the other diagonal direction. This is a limiting case, for if $\tau_{xy}/\sigma_x > 1$, σ_2 is compressive, and the membrane will buckle (wrinkle) in its initial state. Contour plots of mode shapes corresponding to some of the frequencies are shown in **Figure 9**. For $\tau_{xy}/\sigma_x = 1$, the node lines are all straight, and parallel to the direction of the applied principal stress (σ_1).

Nomenclature

h	thickness
T	uniform tension
w	transverse vibrational displacement
α	sector angle
ϕ	arbitrary phase angle

See also: **Plates**; **Shells**.

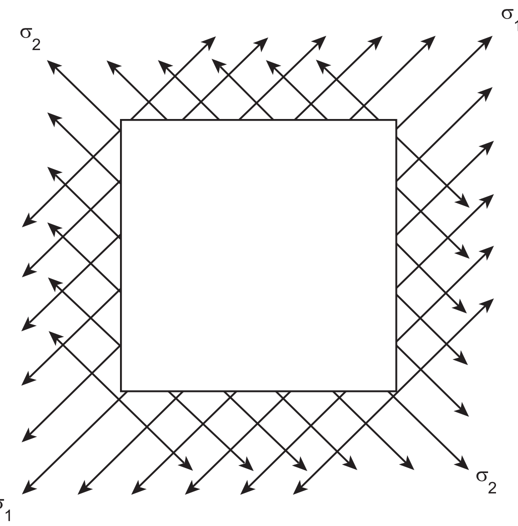

Figure 8 Biaxial diagonal tensile stresses.

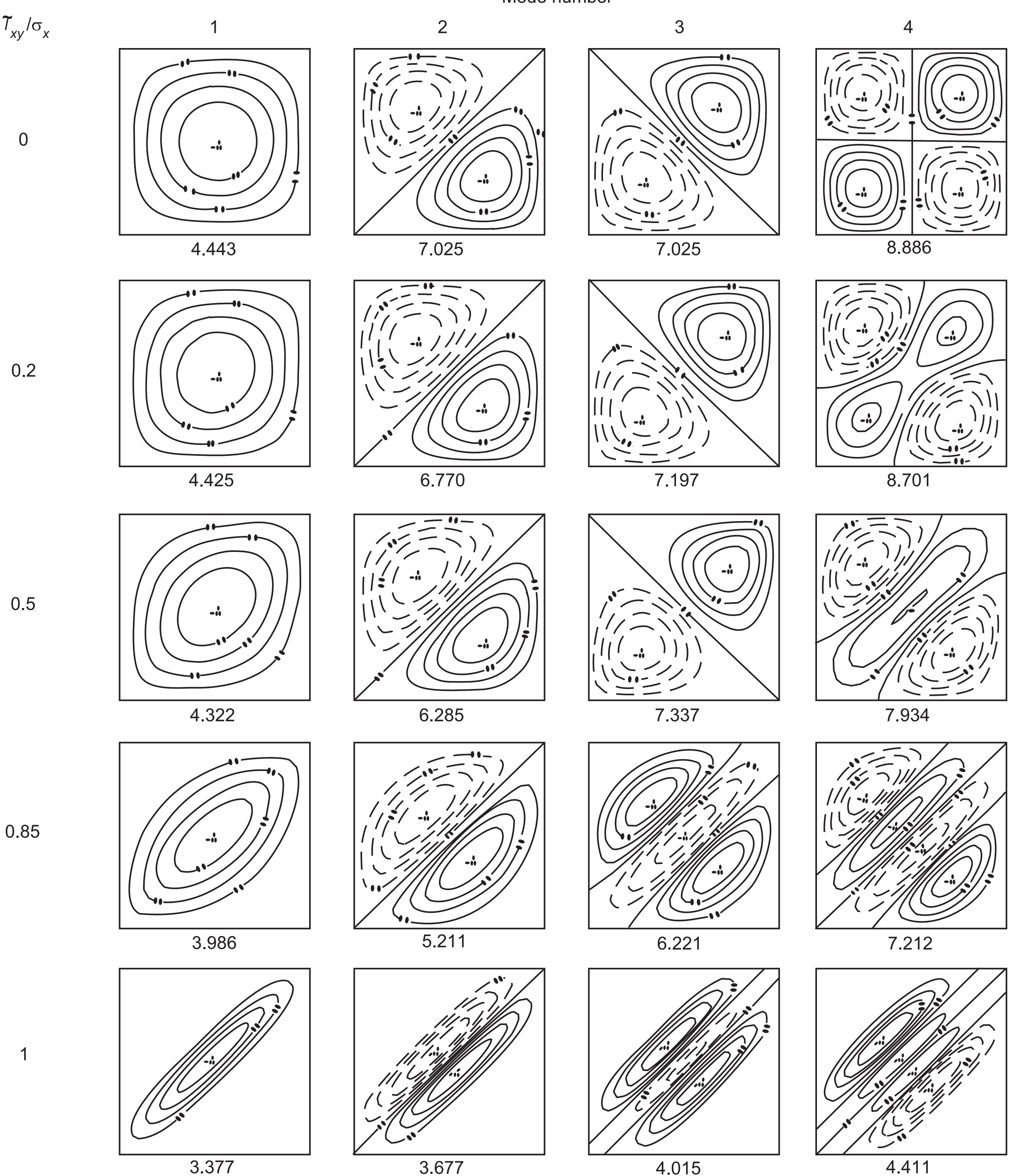

Figure 9 Mode shape nodal patterns corresponding to some of the frequencies in **Table 5**.

Further Reading

Courant R, Hilbert D (1953) *Methods of Mathematical Physics*, vol.1. New York: Wiley Interscience.

Lord Rayleigh (1945) *The Theory of Sound*, vol. 1. New York: Dover Publications (reproduction of 1877 original published by the MacMillan Co.).

Meirovitch L (1967) *Analytical Methods in Vibrations*. New York: Macmillan.

Timoshenko SP, Young DH, Weaver W (1974) *Vibration Problems in Engineering*, 4th edn. New York: Wiley.

MEMS, APPLICATIONS

I Stiharu, Concordia University, Montreal, Quebec, Canada

Copyright © 2001 Academic Press

doi:10.1006/rwvb.2001.0075

Introduction

Microelectromechanical systems (MEMS) applications have been conceived for both substitution and for new products. The decreased cost associated with very large production is directing the utilization of the microsystems into applications that require mass production. Pressure, temperature, proximity, acceleration or chemical integrated microsensors for automotive application represent a large family of substitution MEMS. Intelligent transportation systems (ITS) technology is another motor of development for new microsystems. The health care devices are also regarded as great potential applications for either substitution or new products.

The primary feature of MEMS applications is that they adequately detect and influence phenomena where microscale interactions are adjoining to macroscale effects. The small-size, low-energy consumption endorsed by high reliability, low cost, and capability to process and deliver undistorted measurement signals in a form that the user can easily exploit constitute the major strengths of MEMS. Microsensors usually do not interfere with macrophenomena, while they could track microscale events accurately. MEMS are thus capable of perceiving the nature to a much lower scale size than the normal-sized sensors do. They can be implemented in time-varying spatial microscale configurations to survey the borderline transition from micro to macro phenomena. Thus, applications of MEMS sensors in resonant structures, buckling, turbulent flow, acoustics, thermo-stress phenomena, and phase change, are befitting. The low cost of the microsensors permits allocations of much larger numbers of measurement points in systems that require synchronization of distributed response, in dynamic allocation of scarce resources systems, or in redundant control and decision management systems.

Although the great majority of the present commercially available devices are based on bulk micromachining, surface micromachined microsystems represent the desired turnout for future MEMS. The capability to integrate on the same chip when produced during the same process, the integrated circuit (IC) circuitry, and the sensing/actuating device enable applications that up to now have been unimaginable. The large number of present MEMS-based systems represent just a small fraction of the possible conceivable and unique applications that will be available in the very near future. A number of available applications involving MEMS are shown in **Table 1**. The applications listed are at various levels of development, ranging from laboratory testing to the market. Most microsystems are still related to the macroscopic perception of the world, whereas those conceived to handle the matter at miniature scale have been implemented more recently. DNA-mapping kits and bioanalysis systems on a single chip are an application that will probably soon be commercially available. However, the endowment of MEMS has become quite common, such that the acknowledgment of the microtechnology in newly developed systems is no longer publicized by the manufacturer.

The related applications of MEMS to the dynamics of mechanical systems are mostly limited at this time to those accomplished by the normal-sized sensors. Accelerometers, angular rate sensors, vibrometers, microphones, and pressure sensors, are the most common applications available at this time. There are very few MEMS devices in large-scale commercial use, other than microsensors and microvalves. However, sustained research is being carried out to accomplish fully integrated systems in one single chip. Thus, single-chip autonomous microrobot or computer hard-drive units on a single chip, implantable drug delivery systems equipped with sensors, valve, reservoir, and controller, or ion propulsion miniature systems for space application are only a few of the microsystems which have been thoroughly investigated. If the progress in accomplishing fully integrated microsystems is considered to be moderate, microelements such as new microsensors and microactuator concepts and prototypes are constantly being reported.

Mechanical Microsensors

Most MEMS mechanical sensors are alternatives for existing normal-sized sensors. Regardless of the physical quantity detected, MEMS mechanical sensors

Table 1 Potential applications of MEMS

Area of application	*Application*
Mechanical microsensors	Microaccelerometers
	Microgyroscopes
	Rate, speed, and position linear and angular sensors
	Vibration measurement systems
	Pressure, temperature, flow, gas composition sensors
Fluid control	Microvalves, smart valves
	Micropumps
	Gas/liquid chromatography
	Logic fluidic elements
	Multisensing arrays
Biomedical	Multiple microchemical test kits
	Multisensing and surgery catheters
	Drug delivery
	Cell handling
	Cell fusion
	Biomolecular handling
	Blood test integrated cell
	Multiple virus integrated test kits
Human sensing stimulation	Neural activity detection and measurement
	Tactile stimulation
	Hearing and visual aid
	Smell sensors
	Distributed arrays of multiple sensing
Microoptics	Fiberoptic alignment
	Scanning
	Modulation
	Interferometer
	Optical head
	Optomechanical integrated circuits
	Arrays of mirrors and varying-focal mirrors
Microprobing and microtesting	Atomic force microscopy probes
	Scanning tunneling microscope probes
	Near-field microscopy probes
	Tunneling probe arrays
	Microbalances
Computer/peripheral components	Magnetic, printer, compact disk head
	Laser scan
	Micromechanical memory
Integrated circuit technology	Micromanipulators, microprobes
	Micropositioners
Robotics	Microrobots
	Microteleoperators
	Mobile sensors

exhibit a larger measurement range, higher sensitivity, better linearity, and lower hysteresis. Besides, all commercially available MEMS mechanical sensors easily comply with the rule of 20% for a new product: newly developed MEMS-based products are at least 20% less expensive to build and/or perform 20% better. Many MEMS devices are developed at a cost which is 10 times less expensive and perform 10 times better than normal-sized sensors. The most significant impact of MEMS, however, arises from their applications, which in most cases cannot be realized with normal-sized systems. A multiactive linking catheter, arrayed mirror high-resolution display, or a swimming microrobot represent only a few of the research topics which are most likely to grow into commercial products which will have a large impact on our life.

The automotive industry has had most benefit from MEMS so far. The mass production of cars requires mass production of sensors, which can be made more economical and rugged through micromachining. Research reports predict a growth of the MEMS device industry to about $35 billion annually by the year 2002: more than half of this is attributed to the automotive industry. **Figure 1** illustrates the distribution of MEMS applications on the end-user industry.

Pressure and acceleration sensors have already been successfully implemented as typical MEMS commercial products. The excellent features of micromachined accelerometers enabled a tremendous impact in the improvement of car dynamics. The low mass and reduced power consumption associated with a reduced cost in microaccelerometer have facilitated the implementation of the MEMS structure in various vehicle applications, ranging from air bag deployment system to the active suspension.

Microaccelerometers

Microaccelerometers are miniature inertial masses elastically suspended on inertial frames that are rigidly connected to the body on which the acceleration should be measured. The inertial mass moves in proportion to the acceleration amplitude of the moving body. The amplitude of motion is detected and converted into an electric signal. The lower the mass of the accelerometer, the higher the natural frequency of the microaccelerometer is. Thus, the main requirement for an accelerometer could be accomplished through miniaturization. The natural frequency of microaccelerometers is often beyond 10 kHz, while their mass can be as low as 50 μg.

Such a microsystem is illustrated in **Figure 2**, as an ADXL50 micromachined accelerometer. This is a complete one-axis acceleration measurement system on a single monolithic IC. Detection of acceleration is based on inertial displacement under external acceleration of an elastically suspended mass. The fixed armatures detect both amplitude and direction of the displacement through capacitive measurement with respect to the fixed electrodes. Along with the sensing structure, the chip comprises an oscillator, reference signal circuit, preamplifier, demodulator,

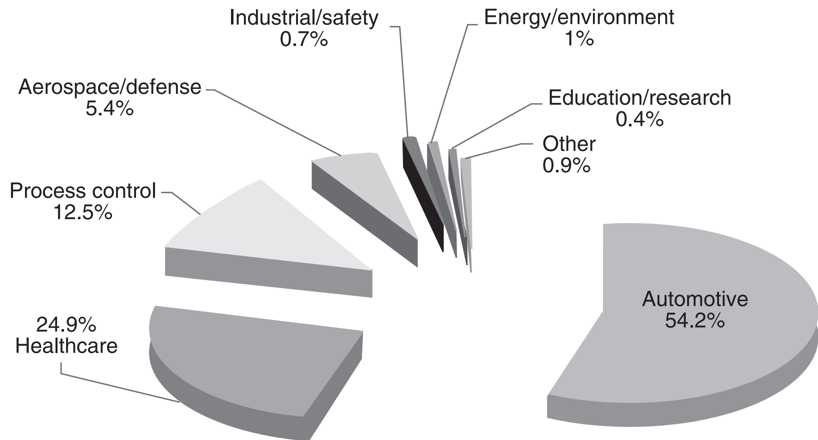

Figure 1 Applications of MEMS and end-user industries.

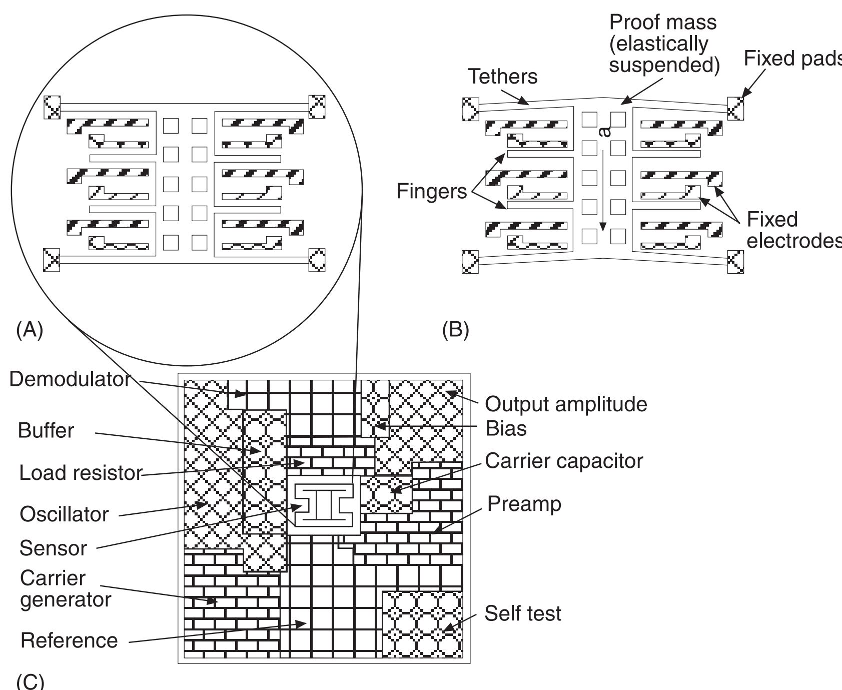

Figure 2 Schematics of the microaccelerometer ADXL50. (A) With no excitation, the proof mass rests in a balanced position. (B) Under the acceleration, the proof mass moves along with the fingers. The relative position of the fingers with respect to the fixed electrodes is related to the magnitude of the acceleration. (C) Schematic view of the entire microsystem.

bias compensation circuit, and self-test circuit. Traditionally, such microaccelerometers have been used in air bag deployment systems. However, other applications in vehicle and seat active suspensions make use of such microaccelerometers. The low cost and high reliability of MEMS represent an important driving factor in the progress of implementation of the intelligent vehicle system (IVS). This concept comprises implementation of sensors and marks, such that roads and vehicles would be able to interact and improving the traffic on congested roads. Proximity sensors, impact avoidance sensors, position and guidance sensors, and remote communication devices are essential elements in the implementation of efficient adaptive traffic schemes on highways. In the vehicle industry, many other solid-state microsystems, such as thermal, optical, magnetic, or chemical sensors, have been implemented and are intensively used. Engine management, wipers, mirrors and lights and air quality control in the car are among the best

known applications of optical and chemical sensors in vehicles. However, such sensors are semiconductor-based devices and do not exhibit any detectable mechanical dynamic outcome. The distinction between solid-state sensors and MEMS is less perceivable from the point of view of function, since most MEMS utilize one or more measurement principles used by solid-state microsensors, such as piezoresistive, magnetoresistive, piezoelectric, capacitive, and ion-sensitive field effect.

One of the most critical problems faced by MEMS is packaging. The diversity of measurands makes package standardization unfeasible for all possible types of microsensors and microsystems. **Figure 3** illustrates a standard packaging configuration that is presently used in IC. Some microsystems require sealed chips, whereas others call for access of the surrounding environment to the sensing area. In certain cases, simple sealed or perforated lids may accomplish specific requirements for specific sensors. In more complex situations, packaging issues are dealt with individually, from case to case. Thus, microactuators may require access to the plant and direct physical contact with the environment. Moreover, rotating parts need protection and lubrication. MEMS devices must also meet the milieu conditions of the application. To illustrate, **Table 2** presents the environmental conditions that a sensor used in the automotive industry must face, as prescribed by SAE J1221 and SAE J5756.

A larger potential of MEMS applications with mechanical microsensors resides in new integrated systems for innovative and emerging applications. As an example, MEMS employed in global positioning systems (GPS) create navigation systems that can provide accurate positioning on a geographic area which are sufficiently accurate to make them appropriate for the ground vehicle traffic management applications. The low cost of MEMS sensors and GPS enables the current implementation of such devices on standard consumer vehicles.

Table 2 Basic requirements for automotive sensors (SAE J1221 and SAE J5756)

Exposure to:	*Range*
Temperature	−40°C to 85°C inside the vehicle −40°C to 125°C under the hood −40°C to 150°C on the engine −40°C to 200–600°C in the exhaust and combustion areas
Mechanical shock	3000 g during assembly 50–500 g in service
Mechanical vibration	15 g, 100 Hz to 2 kHz
Chemical exposure to:	Fuel Oil Freon Humidity Salted water Exhaust gases Ethylene glycol

Since the 1980s the research on MEMS has matured tremendously. The microsystems are permanently heading towards smaller features and integration of mechanical, electrical, and control subsystems on a single chip.

Acoustic Microsensors

The acoustic sensor class exhibits considerable potential for mechanical and chemical sensing. The planar geometry configuration enables compliant fabrication of sensors using standard IC technology. The principle of detection is based on the high sensitivity of the elastic wave velocity, traveling through a resonant media while crossing an active material, which is subjected to excitation from the physical

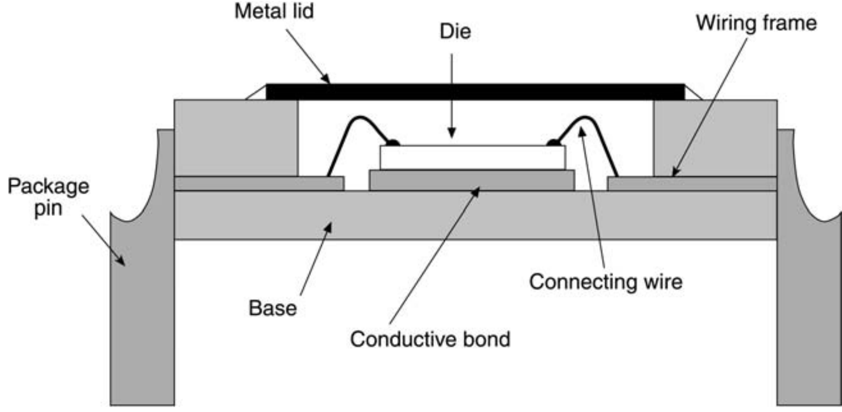

Figure 3 Standard packaging of an integrated circuit.

quantity to be measured. The acoustic wave-based sensors, such as the surface acoustic waves (SAW) and the flexural plate waves (FPW), are based on the piezoelectric properties of classes of monocrystals and ceramics. **Figure 4** illustrates the schematic configuration and functioning of an SAW sensor. One of the SAW interdigital transducers is used to excite the piezoelectric substrate of the sensor. When an electrical charge is applied to a piezoelectric structure, the structure tends to vibrate near its natural frequency or one of its harmonics. The vibration wave propagates through the substrate and travels throughout the coating, which is the active material sensitive to the quantity to be measured. The change in the active material will modify the speed of the crossing wave. The second SAW transducer detects the phase shift or amplitude modification due to the structural changes in the bulk of the sensing material. The acoustic sensors have been known since the early 1960s from their applications with large monocrystalline quartz. The piezoelectric effect can be successfully used in the miniature devices, microsensors, and microactuators. If the structure is a thin plate of mass m and thickness t, the resonance shear-mode wavelength λ (thickness is chosen such that $\lambda = t$) will be modified due to the mass change of the plate by the linear relationship:

$$\frac{\Delta m}{m} = \frac{\Delta \lambda}{\lambda}$$

Modifications to the structure of the delay line will be reflected in the signal perceived at the receiver. This information can always be related to the input excitation, which is directly related to the physical quantity to be measured. The interdigital transducer configuration is very appropriate for MEMS implementation. IC-like technologies have been used to complete monolithic piezoelectric accelerometers along the full scale ranging from 1 to 100 g. The piezoelectric substrate deposition requires some special processing which is not specific to IC processes. Among the thin film piezoelectric materials that can be implemented with IC technology are ZnO, AlN, $Pb(Zr,Ti)O_3$ (PZT), and polyvinylidene fluoride (PVDF).

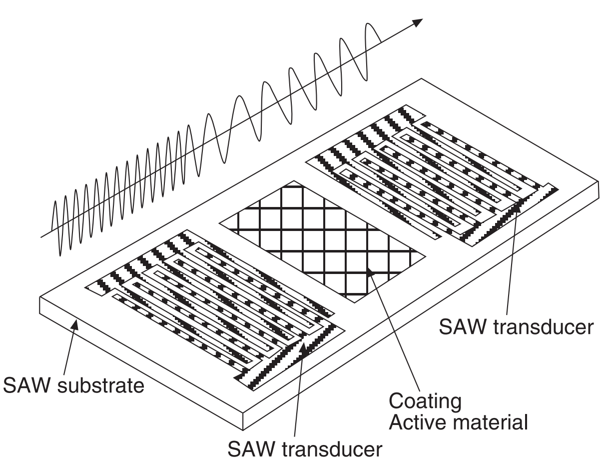

Figure 4 Schematic of a surface acoustic sensor concept. The oscillation generated by the source is changed when passing through the coating which represent the active material. The change is perceived by the surface acoustic wave (SAW) transducer, which detects the change due to the modification in the state of the active (sensing) materials.

Microactuators

Microactuators are conceived to transform various forms of energy, mostly electrical, into mechanical rotation or translation on a miniature scale.

The first electrostatic microactuators were created making use of modified surface micromachining technology in which thick polysilicon rotors actuated by side-driver electrodes were held at the center by a hollow hub. Early designs of micromotors were conceived as small replicas of normal-sized electric motors. At 500 rpm, the life of the motor would not exceed 1 h due to the substantial friction and wear on the sliding surface. Eccentrically rotating motors (wobble motors) were then created to overcome the sliding friction which would be reduced to a roll friction. Moreover, elastically suspended moving elements driven by electrostatic or magnetic fields or actuated by fluid or thermal power have been proposed. Such designs fully eliminate the contact friction.

Some other designs use the friction force between the moving and fixed parts as driving force. Such an example is represented by ciliary motion systems. Miniature actuators making use of piezoelectric, magnetostrictive, or photostrictive or phase transformation effects or thermal effects could generate larger power per mass unit efficiency factors. More creative concepts have been proposed and tremendous progress was achieved in increasing the life of the micromotor and in improving the force/torque. Interdigitated comb-like resonant structures, linear thermal actuators, shape-memory elements, or capillary force-actuated elements are among the many proposed solutions to raise the actuation force of the micromotors. In addition to modified surface machining, high-aspect ratio machining (lithografie galvanik abeforming or LIGA, and deep X-ray lithography) was used to create microactuators. **Figure 5** illustrates the concepts of micromachined actuators. Forces in the range of μN can be accomplished by single microactuators. Optical applications are most

suitable with the force range generated by single unit micromotors. **Table 3** illustrates the work per unit of volume and the frequency range of various classes of microactuators.

Certain macroscopic tasks can be performed by arrays of microactuators. Larger displacements could be achieved by multiple microactuators with synchronized motion, as illustrated in **Figure 5F**, in the case of a ciliary motion conveyer where the actuators are connected in series. Larger loads could also be supported by distributed synchronized micro-actuators connected in parallel. Arrays of microsensors and microactuators connected conveniently in series and parallel can produce higher forces and larger displacements and perform more complex functions than the unit microactuator. Although the energy loss in direct-driven microactuators is minimal, the undesired friction limits the type of

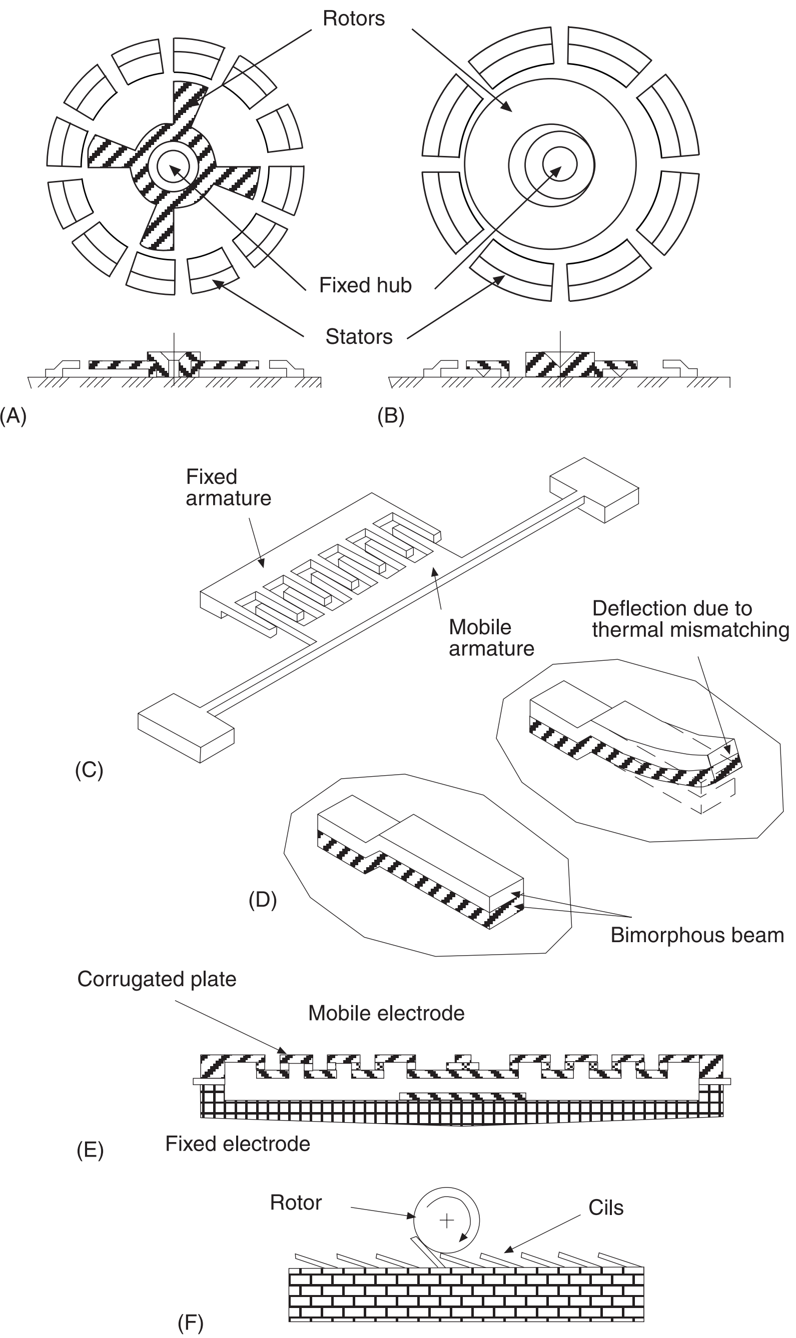

Figure 5 Microactuators. (A) Side-drive electrostatic micromotor. (B) Wobble electrostatic micromotor. (C) Comb-drive microactuator. (D) Thermal actuator (bimorphous cantilever beam). (E) Electrostatic linear microactuator. (F) Ciliary motion conveyer.

Table 3 Work per unit of volume and frequency range for selected types of microactuators

No.	Microactuator type	Work/volume ($J\,m^{-3}$)	Frequency (Hz)
1	Shape memory alloy (Ni-Ti)	$6 \times 10^6 - 25 \times 10^7$	10^2
2	Solid–liquid phase change	4.7×10^6	1
3	Thermal expansion	4.6×10^5	10^2
4	Electromagnetic	$1.6 \times 10^3 - 4 \times 10^5$	10^2
5	Electrostatic	$7 \times 10^2 - 1.8 \times 10^5$	10^4
6	Piezoelectric	$1.8 \times 10^2 - 1.2 \times 10^5$	10^7

transmission elements to the supported beams as linkages. Joints and gears cannot be used in microsystems due to the microscale high friction level that reduces the efficiency of the transmission to values close to zero.

Remarkable applications of microactuators to macroscopic systems have been demonstrated in the control of turbulent flow on surfaces. Augmentation of a disturbance created by a small motion of a microactuator on the surface enable formation of a vortex, which upholds the capability to control the aerodynamic macrophenomena.

Microvalves and Micropumps

MEMS applications in this group are related to fluid handling, chemical analysis, microbiology, aerodynamics, and controls. Early investigations on fluidic microdevices were directed towards the accomplishment of micropumps, microvalves, and shaped flow channels. Most devices have been accomplished through hybrid bulk and special micromachining procedures. Silicon membranes actuated by electromagnetic, electrostatic, or thermal expansion forces have been used as valves, as shown in **Figure 6**. The metallic conductor deposited on the thin membrane will move the flexing element when a current is passed through the coil. The motion can be conveniently used to obstruct one of the valve orifices. Similar structures can be used as a pump if the openings of the two orifices are synchronized. The variation of volume inside the cavity due to the motion of the membrane will induce flow from the input to the output orifices.

Fluidic elements require special packaging such that the moving element is enclosed within a specific structure. Wafer-to-wafer or glass on silicon anodic bonding is usually used to seal the fluidic elements.

Fluidic logic elements have been developed as an alternate solution to the electronic logic circuits. MEMS enable downsizing of these circuits such that full logic controllers can be built on a few square millimeters of wafer. **Figure 7** illustrates such a circuit. The flow stream switches the flow channel if the corresponding control signal is applied through the appropriate control channel.

Chemical analysis integrated systems comprising pumps, valves, sensors, and controllers are under intensive investigation.

Other Applications

Optical microsystems are among the most common applications of MEMS. Here, the mechanical load carried by the actuator is reduced to the intrinsic mass of the moving part. Besides, very performant optical cells can be built in IC technology. Micromachined high-resolution displays comprising arrays of micromirrors, each of 16 μm size, which can be tilted such that the reflected beam creating the pixel image becomes visible or invisible, integrated on metal oxide complementary circuits have been accomplished. Micromechanical optical switches and resonators, optical modulators, tunable filters, or deformable optical wave guides are also available. Applications

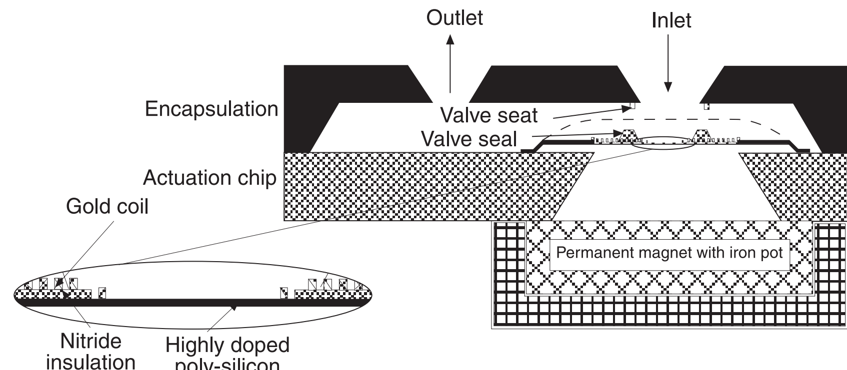

Figure 6 Scheme of a cross-section of the microvalve (actuation chip plus encapsulation and permanent magnet with iron pot).

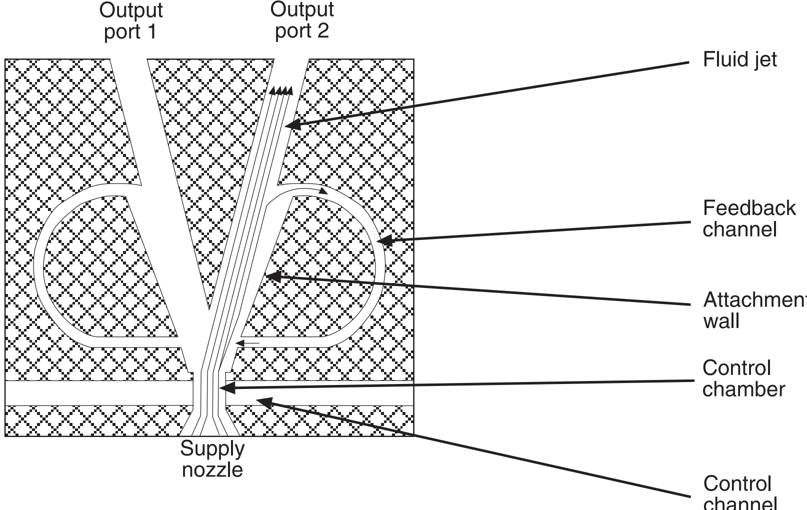

Figure 7 Schematics of a fluidic logic element.

to communications and data storage systems as well as in very high-accuracy measurement devices of the optical MEMS are quite common.

Another type of MEMS application features the investigative systems to nanoscale level of the matter. Thus, scanning tunneling or lateral force microscopy probes and arrays of probes accomplished in silicon dramatically improved the performances of the microscopes, at the same time reducing their cost. The mass of microobjects can be accurately measured, making use of simple principles such as the bending of the free end of a cantilever beam under a gravity force. **Figure 8** illustrates such a measurement system made of an array of beams conceived to measure a larger range of masses.

Biotechnology and medicine also benefit from MEMS. Catheters equipped with micropressure sensors can detect the pressure variation on a portion of an artery, which indicates the existence of clots. Research on similar catheters bearing together with pressure sensors and biochemical sensors that detect enzymes composition and concentration has been carried out. Less invasive probes for tests have been manufactured in MEMS technology and the results obtained claim more effort in developing such systems. Neural probes used to detect the electric potential generated by nerve activity have been built using a hybrid surface and bulk postprocessing of silicon. Such a microelectrode is shown in **Figure 9**. Implantable artificial organs, a microautonomous tool for minimally invasive surgery or drug delivery systems, are among the most desired MEMS due to the enormous positive impact they will have on humans' life.

The ultimate goal of the research effort in MEMS is to create useful micromachines as full systems. Successful applications make use of standard IC processes such that the microsystems could benefit from the coupling of the micromechanical components with the conditioning circuitry and controller on the same miniature unit. Besides, many original systems have been accomplished through bulk micromachining comprising anisotropic Si etching, wafer bonding, and advanced packaging. Since bulk

Figure 8 Microcantilever beam used to scale a small mass. The intrinsic interlayer stress will bend the beam. A micromass is used to bend back the beam. The new value of the deflection is directly related to the mass of the microparticle.

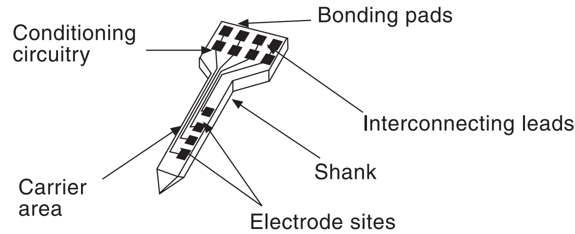

Figure 9 Neural probe.

micromachining could not enable the fabrication of the electronics on the same chip with the microstructure, the circuit is built separately and packaged on the same unit. The variance in sensitivity of the mechanical structure may range within $\pm 20\%$. Compensation is achieved through tuning of the electronic circuitry. Laser trimming as well as look-up compensation tables inscribed in EPROM circuits are compensation methods which are currently used. The low cost and high reliability of microsystems make them serious competitions to the present sensors and controllers. The capability of MEMS to investigate further into the matter of phenomena means that microtechnology has a strong future. Breakthroughs in the following five general areas are predicted to be accomplished by MEMS and MEMS technology:

1. implementation of hierarchic intelligent systems in machines which can analyze, and conclude what the decision is to be taken
2. downsizing and redundancy of systems and deeper investigation of the matter
3. biomimetics: the development of flexible, intelligent, and sensitive autonomous micromachines
4. informatics: the acquisition of information on the state of systems equipped with sensors; exchange of real-time data among interacting systems, decision taking towards the optimization of multiple system functioning
5. environment preservation: measurement, detection, cleaning

MEMS have had, and will have, a profound impact on future technology and society.

See also: **Actuators and smart structures**; **MEMS, dynamic response**; **MEMS, general properties**; **Transducers for absolute motion**.

Further Reading

Bhushan B and Gupta BK (1997) *Handbook of Tribology: Materials, Coatings, and Surface Treatments*. New York: McGraw-Hill.
Campbel SA and Lewerenz HJ (eds) (1998) *Semiconductor Micromachining*. Chichester: Wiley.
Fraden J (1993) *AIP Handbook of Modern Sensors; Physics, Design and Applications*. New York: American Institute of Physics.
Gardner JW (1994) *Microsensors; Principles and Applications*. New York: John Wiley.
Kovacs TA (1998) *Micromachined Transducers Sourcebook*. Boston: McGraw-Hill.
Lee HH (1990) *Fundamentals of Microelectronic Processing*. New York: McGraw-Hill.
Madou M (1997) *Fundamentals of Microfabrication*. New York: CRC Publishing.
Neamen DA (1992) *Semiconductor Physics and Devices; Basic Principles*. Homewood, IL: Irwin.
Ohba R (ed.) (1992) *Intelligent Sensor Technology*. Chichester: John Wiley.
Sze SM (ed.) (1994) *Semiconductor Sensors*. New York: John Wiley.
Tiller WA (1990) *The Science of Crystallization: Microscopic Interfacial Phenomena*. Cambridge, UK: Cambridge University Press.
Weste NHE and Eshraghian K (1994) *Principles of CMOS VLSI Design*. New York: Addison Wesley.

MEMS, DYNAMIC RESPONSE

I Stiharu, Concordia University, Montreal, Quebec, Canada

Copyright © 2001 Academic Press

doi:10.1006/rwvb.2001.0074

Introduction

A microstructure subjected to an input signal would respond with the same oscillation pattern of amplitude that correlates with the characteristics of the structure. Microstructures are particularly associated with high resonant frequencies. This phenomenon is mainly due to the extremely small oscillating masses of the microstructures, but it is also due to the notable influence of the electrostatic and electromagnetic fields, and the built-in interlaminar stress in the structural layers. Detecting the natural resonance frequency of a microstructure in conjunction with the appropriate operating frequency should be considered during the design process.

The dynamic response of microelectromechanical systems (MEMS) involves multiphysics interactions. The association between various physical quantities must be accurately established to evaluate the performance of a microsystem. Geometric downscaling by a factor does not necessarily mean downscaling within the same range for various physical quantities interacting at the microstructure level. For a given one-dimension downscaling factor, the mass and the moment of inertia decrease by the power of 3, the force decreases by the power of 2 and the acceleration grows by the power of 1, while the speed remains unchanged. Such dependence will definitely influence the dynamic response of a miniature structure.

From a dynamic point of view, most existing microsensors (optical, chemical, electromagnetic, temperature, and radiation) are static devices. They usually comprise both the transducer and the circuitry, which are built on the chip or packaged on the same circuit board. Under vibrations, the mechanical structure moves together with the circuitry and the chip. The stiffness of the connections is very high while the free pendent mass of the sensor is very small. Such devices can thus be considered as simple masses. Thus, for most microsystems mechanical vibration has no detectable influence on their functioning. However, the mechanical vibrations could induce quite destructive effects to the package and wire connections on the chip.

The influence of MEMS on the dynamics of the parts supporting the microsystem, on the other hand, is quite negligible. The mass of a standard 3×3 mm silicon chip does not exceed 10 mg, while the mass of a fully packaged chip does not exceed a few grams. Thus, rigid mounting of MEMS to normal-size mechanical systems would not interfere or yield a detectable influence on the overall dynamic response of the mechanical structure under most circumstances.

MEMS comprising flexing or free elements, which are free-standing structures released form the silicon chip by postprocessing, are clamped, supported, or free but constrained in their motion. Such structures are strongly affected by the oscillatory motion induced to their support or foundation. The dynamic response can be roughly modeled as a lump mass–spring–damper system fixed on a vibrating foundation, as shown in **Figure 1**. The motion along the free direction x of the swing mass of the microsystem is described by the force equilibrium equation:

$$m\ddot{x} + c(\dot{x} - \dot{x}_0) + k(x - x_0) = X_0 \sin(\omega t) \qquad [1]$$

The deflection x of the free-standing microstructure follows, after a lag, the pulse of the excitation:

$$x = A \sin(\omega t - \phi)$$

where the amplitude A and phase shift ϕ are given by:

$$A = X_0 \sqrt{\frac{k^2 + (c\omega)^2}{(k - m\omega^2)^2 + (c\omega)^2}} \qquad [2]$$

and:

$$\phi = \tan^{-1}\left(\frac{mc\omega^3}{k(k - m\omega^2) + (c\omega)^2}\right) \qquad [3]$$

The main feature related to the dynamics of MEMS is the high value of the resonant frequency, which is mainly due to the extremely low mass of the microstructure. This attribute makes them valuable measurement tools for high-frequency bandwidth vibrations in mechanical systems.

In the case of microaccelerometers, microvibrometers, atomic force probes, and microphones, the motion of the free-standing element is beneficial and regarded as the measurable input signal, so the structure must always behave in the predicted way. The motion of the free-standing element is further transformed into electric effectual signal. The dynamic behavior of the microstructure must be predicted through modeling, before such a microsystem can be accomplished. The modeling of the mechanical structure often involves fluid, thermal, and electromagnetic interactions. The electrical circuitry requires further attention, since the resonant frequency of the mechanical microstructures is in general very high. The shift in critical natural frequency makes the microsystem exhibit stronger coupling with the electronic circuitry than the

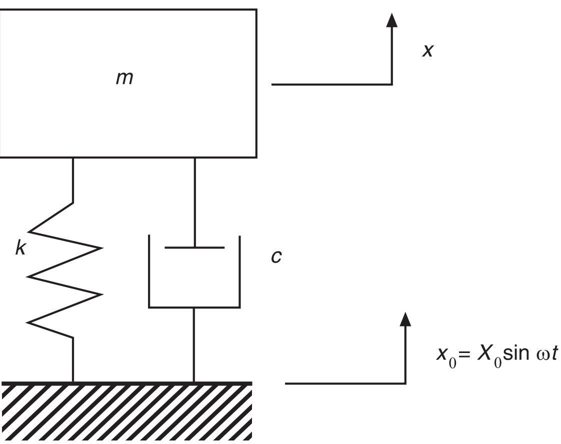

Figure 1 Lump model of damped mass elastically supported on a harmonic vibratory base.

normal-size electromechanical systems. Although MEMS are subjected to multiple physical interactions with very nonlinear effects, the lump mass model is always conceived to estimate the range of the dynamic linear response of the system.

When modeling multiple interactions among the linear physical system, it is perhaps more convenient to convert all the components to one common type of analogous system. Traditionally, all the mechanical, fluid, or thermal elements are converted to standard electrical components. The network models and the analysis methods for the electrical circuits are very popular and intuitive, such that the analysis of the analog systems is notably simplified. Furthermore, software packages can be conveniently used for the equivalent electrical network analysis.

For the normal-size world, **Table 1** gives the equivalent circuit components and signal variables among electrical, mechanical, fluid, and thermal physical quantities. The same analogy can be extended to the microworld, with some reservations due to the major influence of certain phenomena that are significant at a microscale level. However, attention is required when the figure number for the damping or stiffness or even mass is fed into the equation of the model. Moreover, it should be emphasized that microminiature systems usually exhibit noticeable nonlinearities, which should be taken into account when more accurate modeling is carried out.

Dynamic Response of MEMS

MEMS which are structured in micromechanical configurations comprising masses elastically suspended exhibit specific dynamic behavioral patterns similar to those of the normal-sized mechanical systems. The small masses associated with relatively large stiffness bring the resonant frequency of the structure in the range of kHz. However, other forces, which are associated with the processes or with the functioning principles of MEMS, may considerably influence their dynamic behavior. Two of the most significant influences, the electrostatic field and interlaminar stress, will be further discussed. A brief summary that helps to resolve the figure number of mass, stiffness, and damping for the lump model of simple MEMS structures is also given below.

Mass

Mass (the equivalent capacitance in electrical circuitry) can be evaluated assuming the geometry of the feature. However, due to the selectivity of the etchant, the initial shape of the feature may be distorted, as shown in **Figure 2**. The etchant removes the sacrificial film at a high rate but it will also etch from the structural layer to a lower extent. The inner walls of the structural film are sloped after the etching is carried out because the inner walls are gradually exposed to the etchant, whereas the external surfaces are permanently in contact with the etchant and thus uniformly etched. In certain conditions, the density of matter of the thin films is slightly smaller than that of the bulk, so the density figure number should be regarded with some caution. The equivalent mass method stands, when concentrated masses are considered along with the distributed masses.

Table 2 shows the standard formulation for the equivalent mass of cantilever and double-supported beams loaded with concentrated weight. The formulation presented in **Table 2** covers in the first iteration

Table 1 Analogous elements and variables

Electrical	*Mechanical*	*Fluid*	*Thermal*
Current (j)	Force (F)	Volume flow (q)	Heat flow (H)
Potential (V)	Speed (v)	Pressure (p)	Temperature (θ)
Resistance $R=\frac{\Delta V}{i}$	Mechanical resistance (damping) $\frac{1}{b}=\frac{\Delta v}{f}$	Fluid resistance $r=\frac{\Delta p}{q}$	Thermal resistance $R_\theta=\frac{\Delta\theta}{H}$
Inductance $L=\frac{\Delta V}{\mathrm{d}i/\mathrm{d}t}$	Mechanical resistance (spring) $\frac{1}{k}=\frac{\Delta v}{\mathrm{d}f/\mathrm{d}t}$	Fluid inertance (inertia) $L=\frac{\Delta p}{\mathrm{d}q/\mathrm{d}t}$	Thermal inertance — (no significance)
Capacitance $\frac{1}{C}=\frac{\Delta V}{\int i\,\mathrm{d}t}$	Mechanical capacitance (mass) $\frac{1}{m}=\frac{\Delta v}{\int f\,\mathrm{d}t}$	Fluid capacitance $\frac{1}{C}=\frac{\Delta p}{\int q\,\mathrm{d}t}$	Thermal capacitance (thermal mass) $\frac{1}{C}=\frac{\Delta\theta}{\int H\,\mathrm{d}t}$

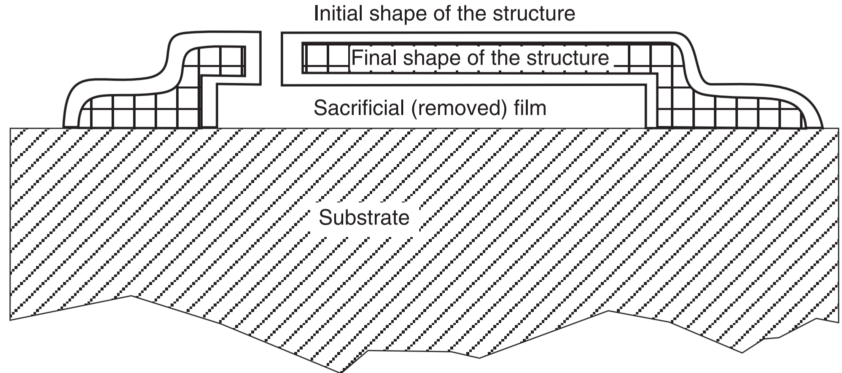

Figure 2 Cross-section through the geometry of a surface micromachined structure transformed due to the limited selectivity of the etchant.

Table 2 The equivalent mass of beams loaded with concentrated mass

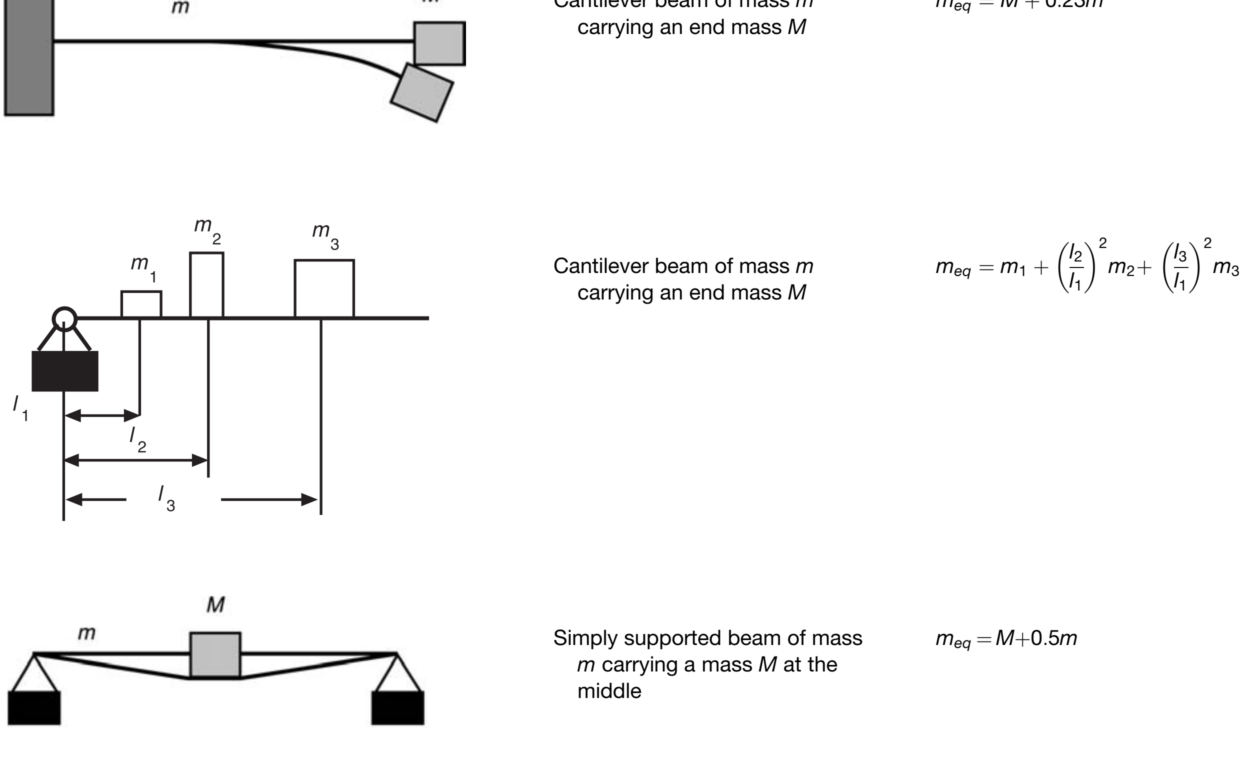

	Cantilever beam of mass *m* carrying an end mass *M*	$m_{eq} = M + 0.23m$
	Cantilever beam of mass *m* carrying an end mass *M*	$m_{eq} = m_1 + \left(\frac{l_2}{l_1}\right)^2 m_2 + \left(\frac{l_3}{l_1}\right)^2 m_3$
	Simply supported beam of mass *m* carrying a mass *M* at the middle	$m_{eq} = M + 0.5m$

most of the MEMS structures, which are conceived as beams simple or double supported.

Stiffness

Stiffness (the equivalent inductance in the electrical circuit) is an essential parameter in the evaluation of the dynamic properties of microstructures. Assuming that the structures have uniform geometric features, the analogy with the helical spring can only be applied for concentrated loading. The stiffness can thus be expressed as the ratio between load and deflection:

$$k = \frac{\mathrm{d}F}{\mathrm{d}\delta} \text{ or, for single concentrated torque,} \quad k_\theta = \frac{\mathrm{d}M}{\mathrm{d}\theta} \qquad [4]$$

When the loading is uniformly distributed on a section of the structure, the equivalent loading method

may be employed to determine the equivalent stiffness. **Table 3** shows the equivalent stiffness for selected types of beams loaded with concentrated and distributed loads.

When the structure is subjected to multiple concentrated loads, the energy method is instrumental in evaluating the equivalent stiffness of the system. The strain energy in the structure is equal to the equivalent energy of a theoretical spring:

$$\sum \left[\int_l \frac{M_b^2 \mathrm{d}x}{2EI} \right] = \frac{k_{\mathrm{eq}} \delta^2}{2} \qquad [5]$$

for bending and:

$$\sum \left[\int_l \frac{M_t^2 \mathrm{d}x}{2GI_p} \right] = \frac{k_{\theta \mathrm{eq}} \theta^2}{2} \qquad [6]$$

for torsion where M_b is the equivalent bending moment in each element of structure, M_t is the equivalent torsion moment in each element of structure, E is the Young's modulus of elasticity, G is the shear modulus of elasticity, I is the moment of inertia of the section of the structure, I_p is the polar moment of inertia of the section of the structure, K_{eq} is the equivalent bending stiffness of the structure, $K_{\theta \mathrm{eq}}$ is the equivalent torsion stiffness of the structure, δ is equivalent deflection of the structure, and θ is the equivalent torsion angle of the structure.

Damping

Damping evaluation requires the most laborious analytical effort. The small geometric size of the flexural elements and the reduced gap between the mobile and fixed part of the structure promote squeeze damping, which can reach remarkably large values of damping coefficients. Damping is critical to the performance of the microsystem throughout the frequency bandwidth of the system. Large values of squeeze film damping, which are likely to occur in MEMS, can reduce the dynamic bandwidth of the system to an unacceptable level. Damping is determined by the geometry of the gap and of the elements, as well as by the viscosity or the pressure of the surrounding fluid. Damping is of great concern for microaccelerometers and miniature microphones. The frequency response of such systems can be improved by reducing damping by configuring flow channels through the flexing or fixed elements or through low-pressure encapsulation. For laterally oscillating microstructures, like comb-like resonant structures, the dominant nature of the damping is due to Couette-type

Table 3 The equivalent stiffness of beams loaded with concentrated and distributed load

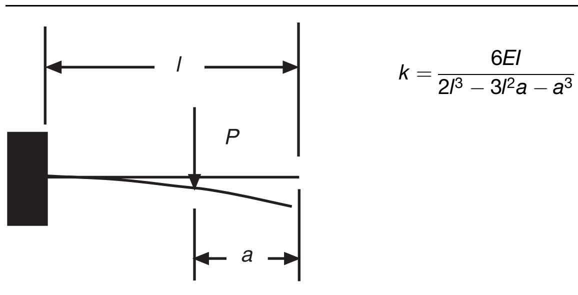

$$k = \frac{6EI}{2l^3 - 3l^2 a - a^3}$$

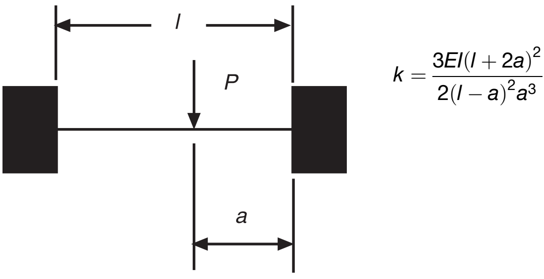

$$k = \frac{3EI(l + 2a)^2}{2(l - a)^2 a^3}$$

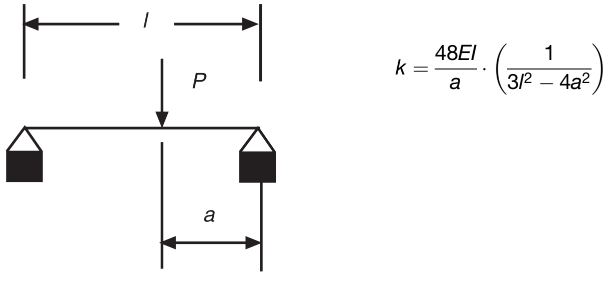

$$k = \frac{48EI}{a} \cdot \left(\frac{1}{3l^2 - 4a^2} \right)$$

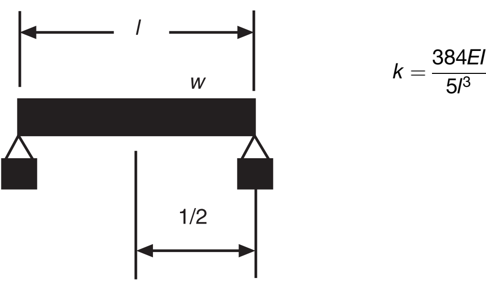

$$k = \frac{384EI}{5l^3}$$

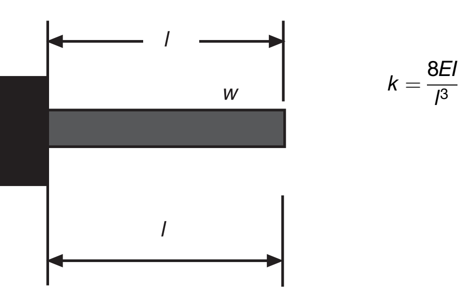

$$k = \frac{8EI}{l^3}$$

flow. **Table 4** gives the equivalent damping values for some energy dissipation arrangements. Reduced damping requires reduced pressure of the immersing fluid/gas.

Certain classes of application require very low damping. The resonant structures (piezoelectric actuators and acoustic sensors) function based on the oscillatory properties of specific active materials (quartz, $LiNbO_3$, ZnO, AlN, PZT, etc.). Low intrinsic damping properties of the material ensure that the system is more efficient through reduced energy dissipation/loss.

When damping is low, the dynamic over the static amplitude ratio at resonance, the quality factor Q, yields considerable information about the dynamic response of the system. The bandwidth of the system represents the range of frequencies for which the amplitude ratio falls beyond $Q/2$. The Q factor of a structure is associated with the ratio of the strain energy stored in the system to the energy dissipated through damping.

When the natural frequency of a more complex system is evaluated, it is more appropriate to use one of the energy methods. One of the remarkable advantages of such a method is that one can incorporate various effects of the electric and magnetic field, and capillary forces, which would otherwise be excessively difficult to incorporate in the model. Equating

Table 4 The equivalent damping for various mechanical structures

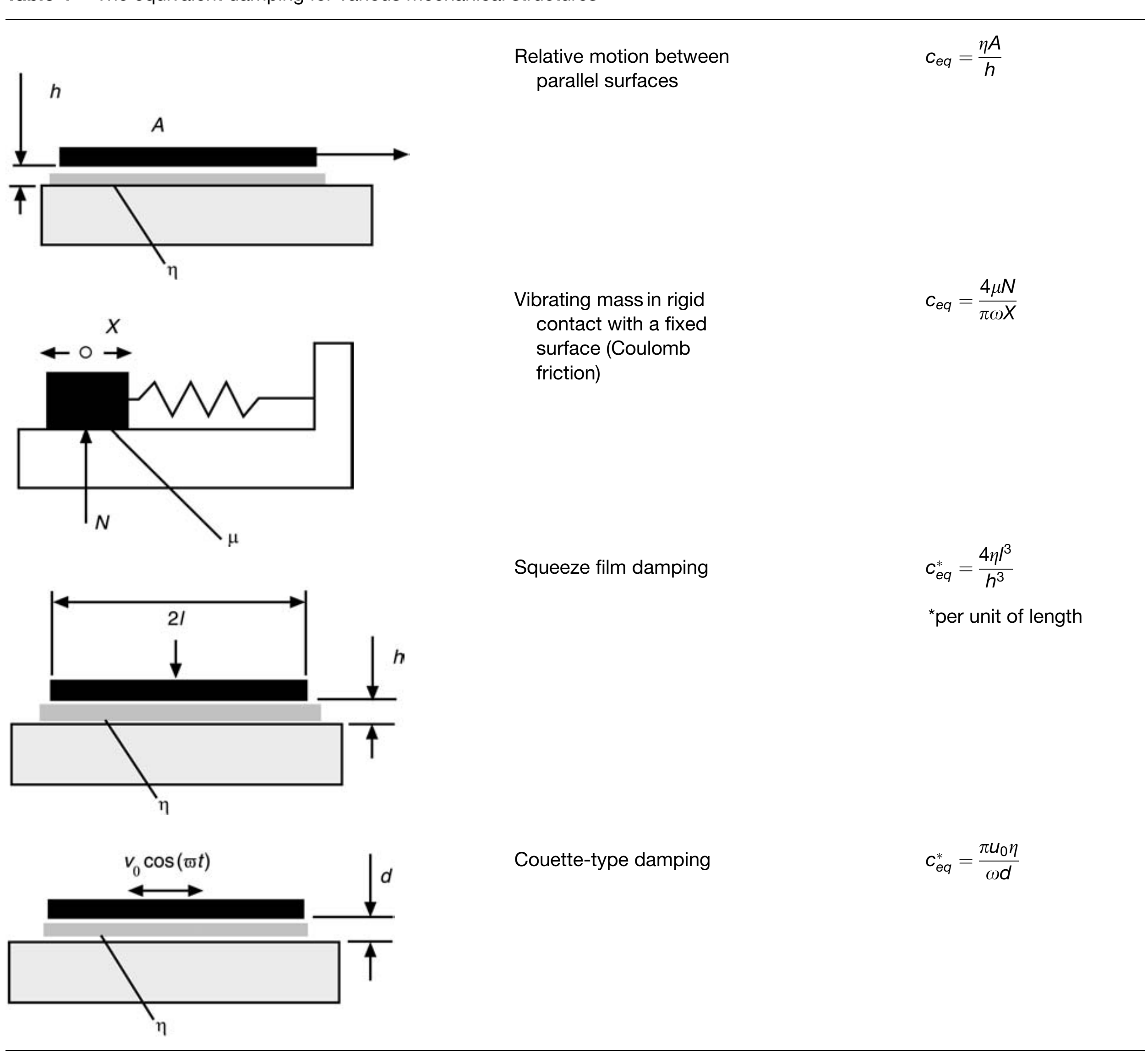

Diagram	Structure	Equivalent damping
	Relative motion between parallel surfaces	$c_{eq} = \frac{\eta A}{h}$
	Vibrating mass in rigid contact with a fixed surface (Coulomb friction)	$c_{eq} = \frac{4\mu N}{\pi\omega X}$
	Squeeze film damping	$c^*_{eq} = \frac{4\eta l^3}{h^3}$ *per unit of length
	Couette-type damping	$c^*_{eq} = \frac{\pi u_0 \eta}{\omega d}$

the maximum potential energy and the kinetic energy, one can assess the influence of the external forces and fields to the natural frequency of the structure.

The Influence of the Electrostatic Field

Assume two parallel plates separated by a small gap. One plate is fixed while the other moves along the direction z normal to the two plates. The mobile plate is subjected to elastic restoring forces. The motion of the plate in the fluid filling the gap between the two plates yields a dissipative force which is proportional to the speed of the plate. The distance between the two plates is usually measured through the value of the impedance of the variable capacitor formed by the two plates. The small size of the micromechanical structures of MEMS enables the electric field which is always present to strongly influence the dynamic response of a microstructure. The energy due to the electrostatic field can be expressed by:

$$-\frac{\partial U}{\partial z} = \frac{V^2}{2}\frac{\partial C}{\partial z} \qquad [7]$$

where U represents the stored electrostatic energy, V is the voltage differential across the capacitor plates, C is the capacitance of the capacitor, and z represents the deflection of the flexible elastic armature of the capacitor.

Eqn [7] shows that enhanced displacement of the mobile armature tends to augment the intensity of the electrostatic field, reducing the gap and increasing capacitance, and this field will incline to pull the flexing element even more. The armature under the electrostatic field thus renders a larger displacement than that experienced in the absence of the electrostatic field, which could be comprehended as negative stiffening of the structure due to the existence of the electrostatic field. It must be noted that the electrostatic field, regardless the potential of the armatures, produces a weakening effect on the stiffness of the mobile plate. However, the detectable phenomenon is the attraction between the two armatures.

It has also been found that each structure exhibits a specific threshold value of static deflection due to the electrostatic force, and, if this is exceeded, the flexible armature becomes dynamical unstable. The mobile armature is perceived to be collapsing on the fixed back-plate. From the point of view of the electrical field, a threshold voltage is associated with each structure, at which pull-in and ultimately snapping occur. Usually, this condition is associated with mechanical failure of the structure, so it must be carefully avoided. The natural frequency of a plate subjected to electrostatic field will drop due to the negative stiffness effect induced by the electrostatic field. When threshold displacement is reached, the natural frequency approaches zero; this is when the balance between positive and negative stiffness is reached. The trend of the natural frequency of a double-supported plate, which is subjected to a potential difference with respect to the fixed armature, is illustrated in **Figure 3**. The natural frequency and the first few resonance frequency and mode shapes for simple stuctures are given in **Table 5**.

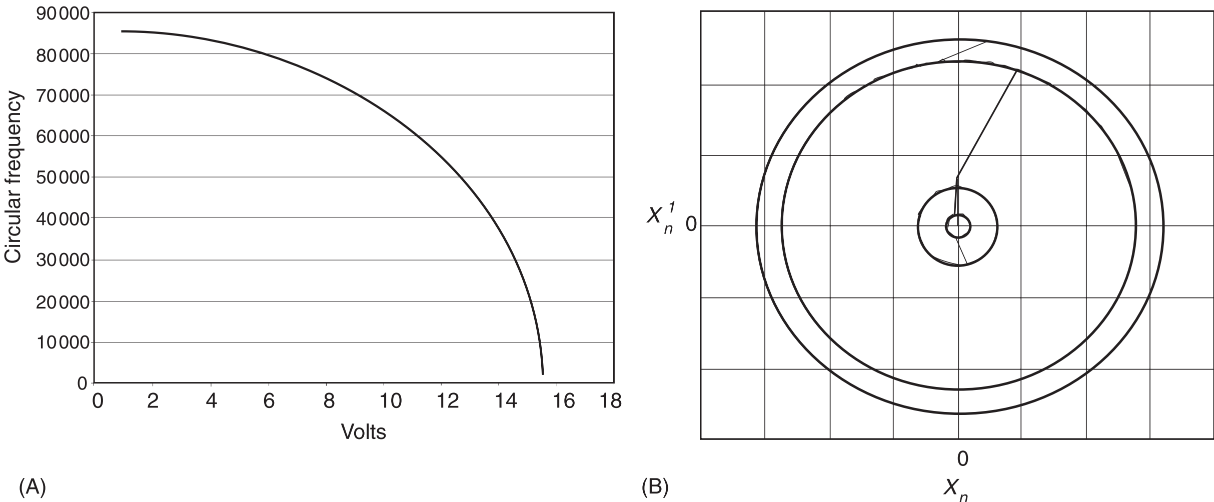

Figure 3 (A) Natural frequency of a microbeam 1000 × 1000 × 2 μm which is double-supported and subject to a variable difference of potential with respect to the fixed armature, parallel and spaced at 2 μm about the beam. The natural frequency decays such that, for voltage beyond 15 V the natural frequency of the plate is close to zero. The plate exhibit dynamic instability at even lower difference of potential, as shown in (B). (B) Phase state plot of the microbeam described in (A), subject to sinusoidal excitation and under an electric field created by 12 V potential difference between the microbeam and the fixed armature.

Table 5 The first resonance frequencies and mode shapes for simple structures.

No.	*Beam configuration*	*Natural frequencies*

1

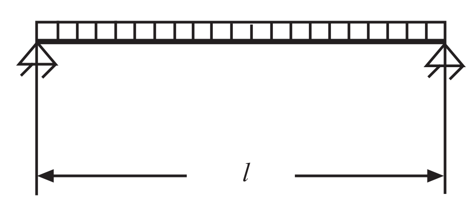

$$f_i = \frac{k_i}{2\pi}\sqrt{\frac{EIg}{wl^4}}$$

Mode	k_i	Nodal position/l
1	9.87	0 1
2	39.5	0 0.5 1
3	88.8	0 0.33 0.67 1
4	158	0 0.25 0.5 0.75 1
5	247	0 0.2 0.4 0.6 0.8 1

2

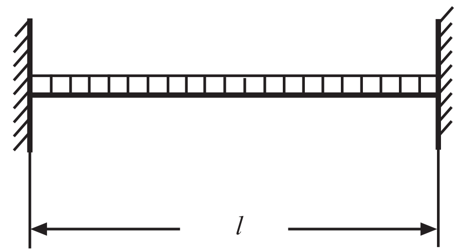

$$f_i = \frac{k_i}{2\pi}\sqrt{\frac{EIg}{wl^4}}$$

Mode	k_i	Nodal position/l
1	22.4	0 1
2	61.7	0 0.5 1
3	121	0 0.36 0.64 1
4	200	0 0.28 0.50 0.72 1
5	299	0 0.23 0.41 0.59 0.77 1

3

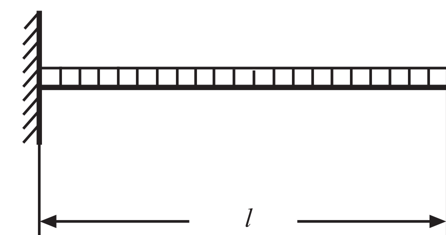

$$f_i = \frac{k_i}{2\pi}\sqrt{\frac{EIg}{wl^4}}$$

Mode	k_i	Nodal position/l
1	3.52	0 1
2	22	0 0.783
3	61.7	0 0.504 0.868
4	121	0 0.358 0.644 0.905
5	200	0 0.279 0.5 0.723
0.926		

4

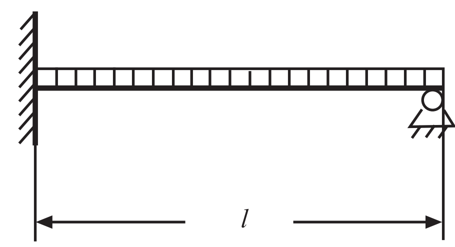

$$f_i = \frac{k_i}{2\pi}\sqrt{\frac{EIg}{wl^4}}$$

Mode	k_i	Nodal position/l
1	15.4	0 1
2	50.0	0 0.577 1
3	104	0 0.386 0.692 1
4	178	0 0.295 0.529 0.765 1
5	272	0 0.239 0.428 0.619 0.810
1		

5

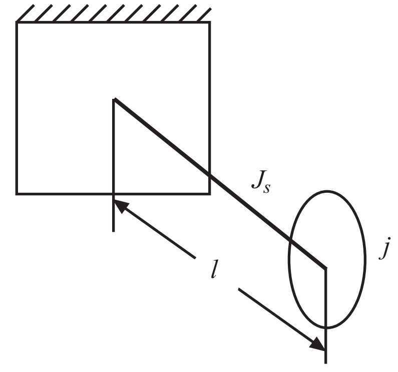

$$f_i = \frac{k_i}{2\pi}\sqrt{\frac{6k_i}{(j + (j_s/3))l}}$$

Mode	k_i
1	1.57
2	4.71
3	7.85

Table 5 continued.

No.	Beam configuration	Natural frequencies
6	$f_i = \frac{k_i}{2\pi}\sqrt{\frac{Tg}{wl^2}}$	Mode / k_i: 4 / π; 5 / 2π; 6 / 3π
7	$f = \frac{k}{2\pi}\sqrt{\frac{Et^3g}{12wa^4(1-\nu^2)}}$	a/b / k: 0.9 / 10.2; 0.8 / 11.3; 0.6 / 12.6; 0.4 / 17.0; 0.2 / 27.8; 0 / 57.0
8	$f = \frac{k_i}{2\pi}\sqrt{\frac{Et^3g}{12wr^4(1-\nu^2)}}$	Mode / k_i: 1 / 10.2; 2 / 21.3; 3 / 34.9; 4 / 39.8

Mode	k_i
4	π
5	2π
6	3π

a/b	k
0.9	10.2
0.8	11.3
0.6	12.6
0.4	17.0
0.2	27.8
0	57.0

Mode	k_i
1	10.2
2	21.3
3	34.9
4	39.8

j, concentrated end-mass moment of inertia; j_s, distributed mass moment of inertia; G, shear modulus of elasticity; T, tension in string; i, the rank of the frequency; f_i, natural frequencies (Hz); k_i, constant; r, radius of the circular path; t, thickness of the plate; l, length of the beam; w, load per unit length (including beam weight); I, area moment of inertia; g, gravitational acceleration; E, Young's modulus of elasticity.

In carrying out the design of capacitive, piezoresistive, or acoustic sensors and actuators, the influence of the electrostatic field on the natural frequency decay of the structure must be carefully considered. Such analysis can be carried out using one of the energy methods (Rayleigh for natural frequency or Rayleigh–Ritz for the first few resonant frequencies). By equating the strain energy with the kinetic energy plus the electrostatic energy, the natural frequency or first few resonant frequencies can be calculated. Finite element analysis (FEA) represents another option in identifying the first few natural frequencies of a complex-shaped structure. Finite element modeling permits complex analysis of multilayered complex shape structures, including stress–strain, dynamic, thermal, or electro-magnetic loading, and even combinations of the above.

The Influence of the Interlaminar Stress

Besides the influence of the potential fields, fabrication of thin films may be responsible for the peculiar dynamic behavior of the microstructures. Thin deposited films induce either compressive or tensile stress, which is mainly due to the thermal mismatching between the substrate and the coating encountered at the low ambient temperatures after high-temperature deposition process. The residual stress may produce unwanted bending, warping, and fracture of the structures. However, the existence of the stress in

structure produces changes in the dynamic behavior of the structure. The amount of change in the dynamic properties depends mostly on the quantity of stress built into the structure. The amount of stress is strongly dependent on the parameters of the deposition process, and the values of such stress can range from a few MPa to a few GPa. The low-stressed films are almost always present when accomplishing surface micromachined structures. Certain sequences of processes and thermal treatments could lower the amount of residual stress to close to zero. The measurement of the residual stress can be carried out using experimental techniques that have been created for various stress ranges and specimen size. For full wafer measurement and stress exceeding 10 MPa, the variation of curvature yields the value of the built-in stress, as given by the relationship (Stoney):

$$\sigma_r = \frac{Et_s^2}{6(1-v)t}\left(\frac{1}{R_i} - \frac{1}{R_f}\right) \qquad [8]$$

where t_s is the thickness of the substrate, t is the thickness of the thin film, R_i is the curvature of the wafer before deposition (expected $R_i = \infty$), and R_f is the curvature of the wafer after deposition.The measurement of the large curvatures is performed with optical stress gauge machines, which can detect large radii of curvature of the substrate before and after thin film deposition.

For stress lower than 1 MPa, buckling of a subset of double-supported witness beams is used to range the compressive stress value in a narrow bandwidth. For the tensile stress, special sets of structures consisting of a ring (Guckel rings) supported by a diameter beam are used to evaluate the built-in stress between the substrate and the film. The witness test structures are made from the thin film deposited on the substrate. The two structures described above are shown in **Figure 4**. The array of structures can be contained within a certain design and the measurement consists of confronting the observation through a microscope with a table illustrating the critical stress in buckling versus the geometric dimensions of the beams. The residual stress can be evaluated out of the critical stress at buckling:

$$\sigma_r = -\frac{\pi^2 h^2 E}{3L^2} \text{ for double-supported beams} \qquad [9]$$

$$\sigma_r = -\frac{\pi^2 h^2 E}{12\zeta(R)R^2} \text{ for Guckel rings} \qquad [10]$$

where h is thickness, L is length, R is radius of the Guckel ring, and $\xi(R)$ is the function of the inner and outer diameters.

The residual stress strongly influences the vibration characteristics of the free-standing structures, which are part of MEMS. Flexing multilayered structures such as microbeams and microplates, as shown in **Figure 5**, tune their dynamic response according to the built-in residual stress. The general equation (Lagrange) describing the plate motion is:

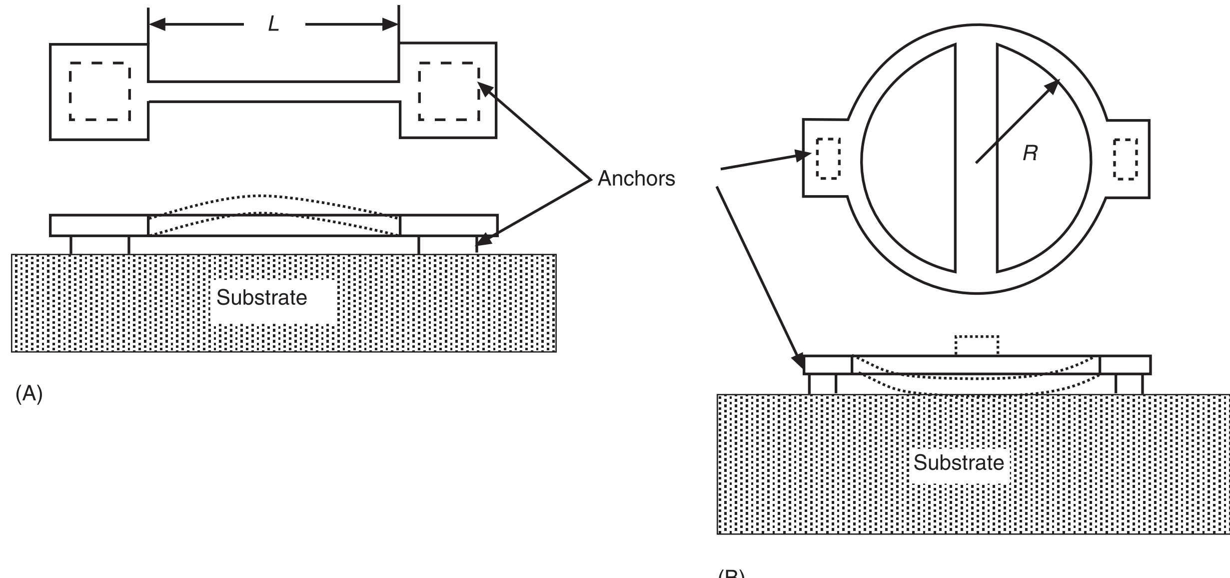

Figure 4 *In situ* structure for low residual stress measurement in thin films. (A) Double-supported beam buckles under compressive stress. (B) Gluckel ring configuration; the diameter beam buckles under the tensile stress in the ring.

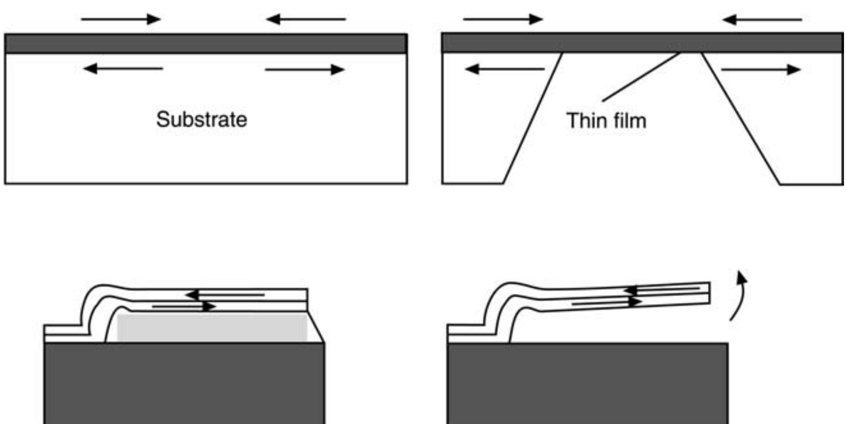

Figure 5 Mismatching stress at the thin film interface. When the substrate or the sacrificial film is etched out to reveal the microstructure, the contour stress or the built-in stress at the interface of the bimorph film will modify the static and dynamic response of the structure.

$$D\nabla^4 z + \rho \frac{\partial^2 z}{\partial t^2} = 0 \qquad [11]$$

with:

$D = \dfrac{Eh^3}{12(1-v^2)}$ flexural rigidity of the plate

∇^4 $\dfrac{\partial^4}{\partial x^4} + 2\dfrac{\partial^4}{\partial^2 x \partial^2 y} + \dfrac{\partial^4}{\partial y^4}$

ρ mass by surface unit

If the plate is subjected to stress, which is equivalent to the stress yielded by the contour lineal forces N_x, N_y, and N_{xy} the previous equation changes to:

$$D\nabla^4 z + \rho \frac{\partial^2 z}{\partial t^2} = N_x \frac{\partial^2 z}{\partial x^2} + 2N_{xy}\frac{\partial z}{\partial x \partial y} + N_y \frac{\partial^2 z}{\partial y^2} \qquad [12]$$

The eigenfrequencies f_i of the plate not subjected to any stress are given by:

$$f_i = \frac{1}{2\pi}\frac{\lambda_i}{a^2}\sqrt{\frac{D}{\rho}} \qquad [13]$$

The eigenvalues of the plate subjected to decoupled lineal forces N_x and N_y ($N_{xy} = 0$) are given in the form:

$$\lambda_{si}^2 = \lambda_i^2 + \frac{a^2\pi^2}{D}\left[N_y m^2 + N_x n^2 \left(\frac{a}{b}\right)^2\right] \qquad [14]$$

From the above last two equations, one can identify the set of lineal forces N_x and N_y which satisfy the relationships:

$$4\rho a^2 \left(f_i^2 - f_{si}\right) = N_y m^2 + N_x n^2 \left(\frac{a}{b}\right)^2 \qquad [15]$$

where f_i is eigenfrequency of the unstressed plate, f_{si} is eigenfrequency of the stresses plate, a, b is dimensions of the sides of the plate, h is thickness of the plate, and m, n are mode numbers.

The last relationship can serve to solve the inverse problems, which are of practical interest. When the stress at the interface of the substrate with the thin layer is known, the shift in the vibration frequencies of a given structure can easily be predicted.

Microplates subjected to forced vibration will thus behave similarly, with the exception that their natural frequency is much higher than that of the normal-sized plates.

Annealing performed on the structures at 800–1000°C in inert gases for 2–4 h can substantially reduce residual stress. However, such treatment is too severe for the electronic circuit components and it can only be applied in the very early stages of a standard integrated circuit process, before the definition of the semiconductor junctions.

Signal Conditioning

Microsensors like any other sensors, must convert the measured physical quantity into meaningful signals. The function of the signal conditioning circuitry consists of converting the sensor output into convenient electrical signals that can be further streamed to the controller or to the data acquisition system. The output signal of the sensor should be a voltage waveform, which can be easily processed by the data acquisition circuit. The process of converting the output signal from the sensor to a voltage can be used to reduce the noise or partially to compensate

for the objective errors collected by the signal from the transducer to the conditioning circuitry.

The new generation of sensors is conceived to comprise on the same chip the signal-processing circuit, the analog to digital converter (A/D), and dedicated controllers. The resolution of the A/D can be maximized by matching the dynamic range of the input signal to the dynamic range of the data acquisition system. The source impedance of the input signal must be low, such that changes in the impedance of the data acquisition system or controller do not affect the signal. The sampling rate of the A/D must be at least twice as fast as the bandwidth of the output signal of the sensor (practically, one order of magnitude higher yields a reasonably accurate conversion).

The output signal of the sensor may include noise that must be removed before it is fed to the A/D. The noise is often associated with stray capacitance of the connection line of the circuit. The high level of integration in MEMS presents the advantage of low-level noise in the signal. However, the electrostatic of the electromagnetic fields may negatively influence the performance of the conditioning circuitry. This problem can be addressed through appropriate packaging of the integrated microsensor.

The output signal of the microsensor may not always match the required input signal of the conditioning circuitry. Thus, appropriate conversion of the signal may be required before being fed to the A/D. The conversion is carried out from voltage, current, resistance, and capacitance, to voltage. Most common conversion schemes are briefly presented below.

Voltage-to-voltage Conversion

Voltage-to-voltage conversion is required when dynamic range modifications (bandwidth reduction or impedance alteration) are necessary, when the output signal from the sensor is a voltage. The abovementioned conversions are carried out by standard circuits. The amplifiers are used to match the output level of the sensor to the input of the data acquisition system. Some of the standard circuits, their scheme, the function carried out and their main properties are shown in **Table 6**. The output signals from the sensor can collect noise. If the frequency of the noise is off the frequency of the significant signal, the unwanted signal can be filtered out using low/high-pass filters. The filtering is usually applied before the signal is amplified. The DC component of the signal, if any, can be removed with an offset circuit.

Current-to-voltage Conversion

Current-to-voltage conversion is usually performed with an operating amplifier in an inverting configuration, since noninverting amplifiers draw very low current. This configuration scheme is most suitable with current-generating sensors. When the current output increases, the output potential increases proportionally.

Resistance-to-voltage Conversion

Resistance-to-voltage conversion is used when the sensor detects the electric resistance variation due to the input signal. Piezoresistive accelerometers, pressure sensors, or microphones are examples of such types of sensors. The resistance variation needs to be translated into standard voltage output to feed the A/DC, the data acquisition circuit, or the controller. The two basic methods to convert resistance variation to voltage output are presented below. The simplest way consists of applying a voltage to a resistor divider network made of the variable resistor R_S (the transducer) and a reference fixed resistor R_R, as shown in **Figure 6**. The voltage detected across the sensor is amplified before being converted to digital signal. The drawback of this method is that the amplifier boosts the entire voltage across the sensor, which translates through a high DC offset. Thus, the second method of converting the resistance to voltage addresses this disadvantage. The resistance bridge configuration, as shown in **Figure 7**, only amplifies the change in voltage due to the shift in the resistance of the sensor. The resistance bridge presents the advantage of zero offset, high sensitivity, and thermal compensation.

Capacitance-to-voltage Conversion

Capacitance-to-voltage conversion is used when the output from the transducer is a variation of capacitance. The capacitance-based sensing presents multiple advantages. The capacitance varies in proportion to the distance between the armatures of the capacitor. The capacitors are sensitive to the material that resides between their electrodes. The most popular methods used to convert capacitance to voltage are similar to those used to measure resistance. However, besides these methods, more innovative principles and circuits have been created. For example, the charge amplifier circuit is used to detect small capacitance variations in the *fF* range.

The voltage divider uses the variable capacitor and a reference capacitor. The circuit configuration is the same as the resistance voltage divider: the only difference is that, instead of the resistors R_S and R_R, capacitors are used. Similarly, the capacitor bridge circuit configuration looks like the resistance bridge in which resistors are replaced by capacitors.

Table 6 Standard circuits

Circuit	*Scheme*	*Input–output relationship*	*Characteristics*
Amplifier inverter	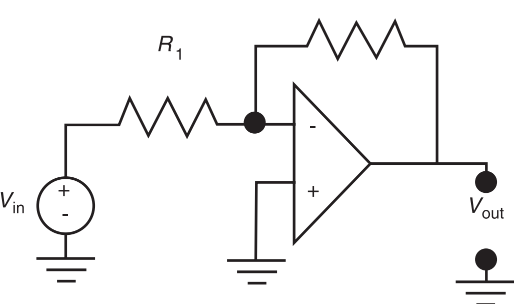	$V_{out} = -\frac{R_2}{R_1} \cdot V_{in}$	Input Impedance $\sim R_1$ Output Impedance ~ 0
Amplifier noninverter	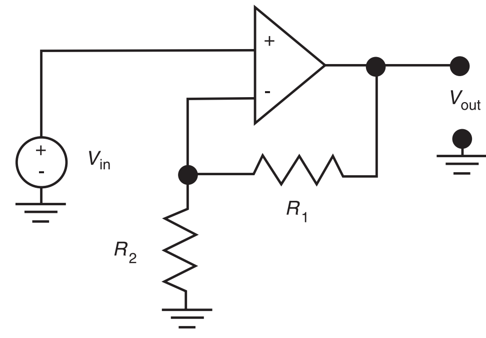	$V_{out} = \left(1 + \frac{R_1}{R_2}\right) \cdot V_{in}$	Input Impedance $\sim \infty$ Output Impedance ~ 0
Summing	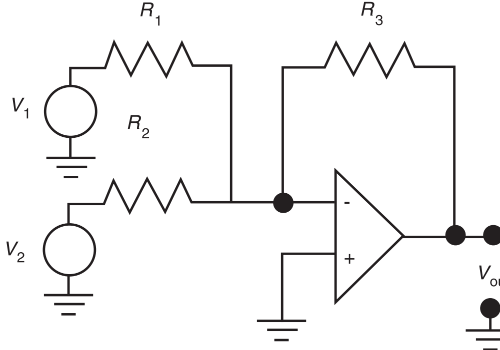	$V_{out} = V_1 \frac{R_3}{R_1} + V_2 \frac{R_3}{R_2}$	Combines the output of arrays to sensors

Table 6 Continued

Circuit	*Scheme*	*Input–output relationship*	*Characteristics*
Difference		$V_{out} = (V_2 - V_1) \cdot \frac{R_2}{R_1}$	Removes unwanted DC offset
Single-pole low-pass filter		$A = -\frac{R_2}{R_1}\frac{1}{1 + j(f/f_o)}$	$f_o = \frac{1}{2\pi R_2 C}$
Single-pole high-pass filter		$A = -\frac{R_2}{R_1}\frac{j(f/f_o)}{1 + j(f/f_o)}$	$f_o = \frac{1}{2\pi R_1 C}$

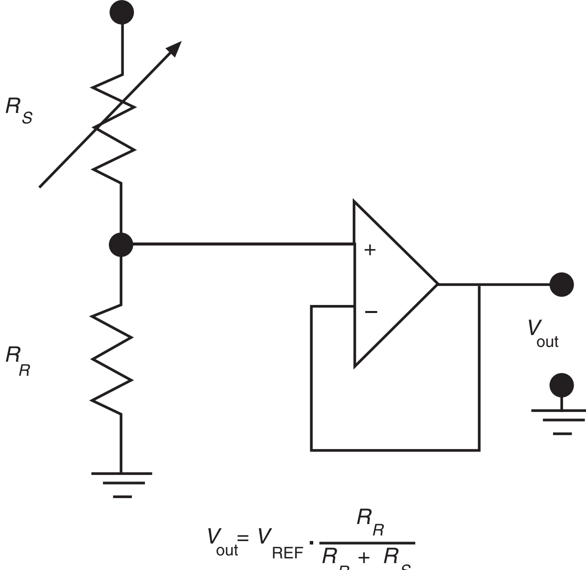

Figure 6 Resistance voltage divider measurement scheme.

The reference signal is sinusoidal, since the capacitance obstructs DC. The impedance of the capacitor is inverse in proportion to frequency. An appropriate reference frequency yields a voltage across the capacitor that is suitable for amplification. When the reference frequency is too low, the high impedance of the sensor creates high levels of noise. When the reference frequency is too high, the low impedance of the sensor allows the sensor to saturate the circuit.

The main feature of MEMS containing free-standing elements is the high natural frequency exhibited by the mechanical structure that may be strongly coupled with the electrical circuit system. MEMS perform in a very nonlinear way in dynamic characteristics. However, in a first approximation, lump mass linear models of the miniature microsystems are satisfactory. Simple formulations of the equivalent mass, stiffness, and damping are analogous with the formulations used in normal-sized systems. For a more accurate analysis of either a simple flexing structure or complex microactuators, the nonlinear phenomena must be considered and examined. They include, but are not limited to, electrostatic and electromagnetic fields, capillary forces, and interlayer mismatch stress. Analysis of the influences of nonlinear physics on the dynamics of the microstructure may be carried out using standard energy methods.

Nomenclature

A	amplitude
C	capacitance
E	Young's modulus of elasticity
g	gravitational acceleration
G	shear modulus of elasticity
h	thickness
I	inertia
L	length

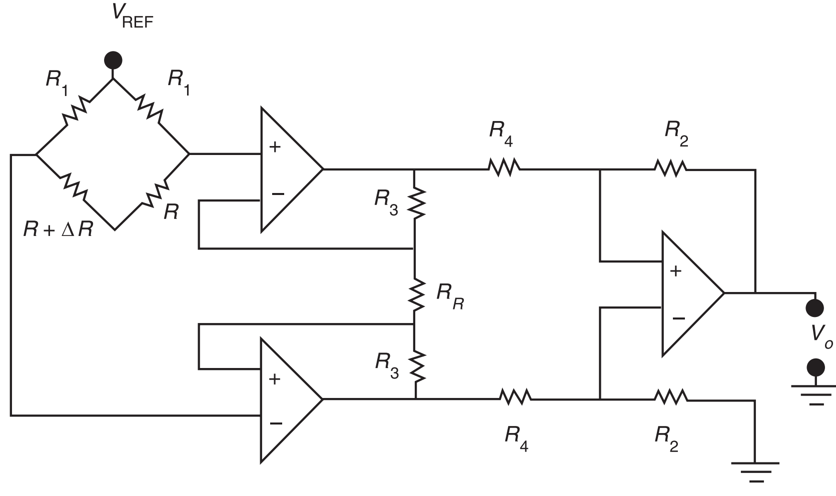

$$V_o = \left(1 + 2\frac{R_3}{R_R}\right)\left(\frac{R_2}{R_4}\right)\frac{R}{R_1 + R} \cdot \frac{\frac{\Delta R}{R}}{1 + \frac{R}{R_1}\left(1 + \frac{\Delta R}{R}\right)} V_{REF}$$

Figure 7 Resistance bridge measurement scheme.

Q	quality factor
R	radius
R_R	reference fixed resistor
R_S	variable resistor
T	tension
U	electrostatic energy
V	voltage
ϕ	phase shift
ρ	mass by surface unit

See also: **Damping materials**; **Dynamic stability**; **MEMS applications**; **MEMS, general properties**; **Signal integration and differentiation**.

Further Reading

Bhushan B and Gupta BK (1997) *Handbook of Tribology: Materials, Coatings, and Surface Treatments*. New York: McGraw-Hill.

Campbel SA and Lewerenz HJ (eds) (1998) *Semiconductor Micromachining*. Chichester: Wiley.

Fraden J (1993) *AIP Handbook of Modern Sensors; Physics, Design and Applications*. New York: American Institute of Physics.

Gardner JW (1994) *Microsensors; Principles and Applications*. New York: John Wiley.

Kovacs TA (1998) *Micromachined Transducers Sourcebook*. Boston: McGraw-Hill.

Lee HH (1990) *Fundamentals of Microelectronic Processing*. New York: McGraw-Hill.

Madou M (1997) *Fundamentals of Microfabrication*. New York: CRC Publishing.

Neamen DA (1992) *Semiconductor Physics and Devices: Basic Principles*. Homewood, IL: Irwin.

Ohba R (ed.) (1992) *Intelligent Sensor Technology*. New York: John Wiley.

Sze SM (ed.) (1994) *Semiconductor Sensors*. New York: John Wiley.

Tiller WA (1990) *The Science of Crystallization: Microscopic Interfacial Phenomena*. Cambridge, UK: Cambridge University Press.

Weste NHE and Eshraghian K (1994) *Principles of CMOS VLSI Design*. New York: Addison Wesley.

MEMS, GENERAL PROPERTIES

I Stiharu, Concordia University, Montreal, Quebec, Canada

Copyright © 2001 Academic Press

doi:10.1006/rwvb.2001.0073

Introduction

MEMS, the acronym for Micro-Electro Mechanical Systems, represents an emerging technology through which miniature mechanical systems are built making use of the standard Integrated Circuits technologies on the same chip as the electronic circuitry. Micromechanical structures along with afferent electronic circuitry often perform functions with high accuracy, which cannot be accomplished by so called 'normal' sized structures. The strength of MEMS is provided through the high effectiveness of the fabrication process, which yields uniform performances for the structures at a relatively low cost, in conjunction with the low power consumption. Moreover, microstructures may probe into phenomena deeper than actual electromechanical systems do.

Microelectromechanical systems (MEMS) are miniature mechanical devices built from silicon using solid-state technology; they contain the necessary electronic circuitry built on the same chip with the mechanical structure. These devices are also known as microsystems or micromechatronic devices. Monocrystalline silicon is a very attractive mechanical material which, in addition to its enabling electrical properties, exhibits remarkable mechanical properties. The elastic modulus is close to that of steel while the specific mass is about three times lower. Silicon enables the parallel batch fabrication of microsystems, which yields higher reliability of the devices together with a dramatic drop in the fabrication cost. The concept of MEMS emerged from the need for miniaturization of the mechanical sensing elements, enabled by the anisotropic crystallographic etching properties of silicon and driven by the enormous progress made in integrated circuits (IC) technology over the last two decades. The field of MEMS has been acknowledged at the end of the 1980s, although the roots of silicon-based sensors and actuators go back to the 1970s.

MEMS are classified into two large functional classes: microsensors and microactuators. Microsensors are conceived as fully signal-conditioned transducers that provide the same function as the classic sensors along with their conditioning circuit board. Since the main functions of sensors are detection and measurement, they should interfere as little as possible with the environment, except for measured

physical quantity. Thus, the energy exchange between the environment and the microsensor should be minimized. Miniature transducers easily comply with these requirements.

Microactuators are conceived to convey energy to their surrounding environment. Their size limits tremendously their performance and thus, the area of application is mainly reduced due to their limited energy storage capability. Arrays of microsensors and microactuators together with implemented controls enable the creation of 'smart matter', which represents a natural step in the development of technology.

The first silicon-based miniature devices were produced in the early 1970s through bulk micromachining. This fabrication principle takes full advantage of batch fabrication but the minimum feature size is limited to fractions of millimeters. Besides, bulk micromachining cannot enable full implementation of the electronic circuitry with the mechanical component on the same silicon chip, using a unique processing flow. The earlier devices thus involved considerable efforts in assembling and packaging the mechanical components and the electronic conditioning circuitry. Further, the research focus has been directed towards developing a comprehensive technology to realize both the reliable electronic circuits and robust mechanical structures integrated within a single design. Attempts to fabricate mechanical devices using modified standard IC processes were successful, so that the conditioning circuitry could be included on the same chip and fabricated during the same process flow. The surface micromachining processes yield a minimum feature size in the range of micrometers. Here, superimposing several patterned layers of conducting, insulating, and transistor-forming materials to build the structural and the sacrificial configurations along with the conditioning circuitry enables the realization of MEMS structures. After the completion of both mechanical structure and electronic circuitry, a sacrificial etching is performed to release the free-standing structure without affecting the function of the electronic circuitry. This step, called postprocessing, requires highly selective etchants and a series of precautions in order to retain the integrity of the microstructure.

The feasibility of the microactuators and micromechanisms has been established through a hybrid technology that enables surface micromachined MEMS based upon thicker polysilicon as the structure and SiO_2 as sacrificial films (MUMPS).

Figure 1 illustrates the difference between bulk and surface micromachining. The bulk-micromachined structures are obtained by removing the excess from

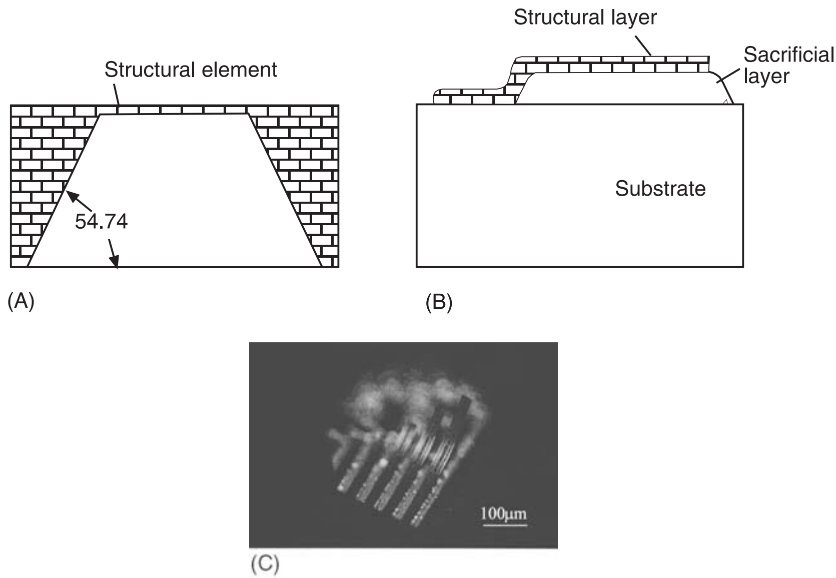

Figure 1 (A) Bulk-micromachined plate in section. The structural element is built from silicon substrate by deep crystallographic anisotropic etching. (B) Surface micromachined step-up free end beam in section. The structural element is built in the top of the sacrificial film. Postprocessing will remove the sacrificial film and release the free-standing structure. (C) Surface-micromachined microbeams released by postprocessing. Mismatching between the materials constituting the polymorphous beams induces high stress which has evolved into spectacular bending of the beam.

the substrate material, such as that shown in **Figure 1A**, through isotropic or anisotropic etching of the material. Surface micromachining yields microsystems enabled by the structural layers deposited and patterned in a specific sequence with the sacrificial layers. The sacrificial layers are removed during postprocessing and the microstructure is released as illustrated in **Figure 1B**. **Figure 1C** shows a magnified picture of a set of micromachined cantilever beams, which are released through postprocessing etching. Thermal mismatching in thin films of various materials, which constitute the beam as a composite material, induces high stresses, resulting in a dramatic bending of the free end of the beam.

Sensors and microsensors are conceived to detect and measure electrical, chemical, magnetic, mechanical, radiant, and thermal measurands. The most common physical quantities and measurands are given in **Table 1**. However, mechanical microsensors are the most interesting from the point of view of vibration. They modify mechanical measurands in electrical signals, using resistive, capacitive, inductive, piezoelectric, or other physical conversion principles.

The primary sensing element is usually a simple elastic structure such as a cantilever beam, which deflects under input measurand. This deflection, although small, is related to the input measurand, which is detected and translated into an electric signal by the built-in subminiature secondary sensing devices, such as piezoresistive, piezoelectric or capacitive elements. The rendered electric signal must be well shielded from the noise of the environment for further conversion into a meaningful indication by the conditioning circuitry. The sensitivity of the sensing element to the measured signal must be high, while sensitivity to irrelevant excitations should be as low as possible. Limitations in sensitivity are related to the measured range and the maximum permitted overloading.

The force/position feedback servosensors structure is more complex, since they comprise both microsensors and microactuators. When distorted by the input signal, the sensing element is returned to its static position by actuators, which are fed by the feedback signal. The signal used to restore the position of the element is meanwhile used for measurement, as shown in **Figure 2**. Such a design concept, although more complex, addresses issues related to overloading and hysteresis.

Table 1 The most common measurands for microsensors

Physical quantity/ measurement principles	*Measurand*
Mechanical	Acceleration, velocity, position
Elastoelectric	Force, moment
Elastomagnetic	Stress, pressure
Thermoelastic	Strain
Thermoelectric	Mass, density
Photoelectric	Flow, flow speed
Photoelastic	Stiffness
	Viscosity
	Energy
Acoustic	Wave amplitude, wave velocity, wave phase
Elastoelectric	Polarization
Elastomagnetic	Frequency spectrum
Photoelastic	Intensity
Magnetoelectric	Energy
Thermal	Temperature
Thermoelectric	Thermal flux
Thermomagnetic	Specific heat
Thermoelastic	Thermal conductivity
Thermooptic	Thermal energy, thermal power
	Energy
Electrical	Charge, current
Magnetoelectric	Potential
Thermomagnetic	Electric field
Thermoelectric	Conductivity
Photoelectric	Permittivity
Elastoelectric	Energy
Magnetic	Magnetic field
Magnetoelectric	Magnetic flux
Elastomagnetic	Permeability
Thermomagnetic	Energy
Optical	Wave amplitude, wave velocity, wave phase
Photoelectric	Polarization
Photomagnetic	Frequency spectrum
Photoelastic	Energy
Radiation	Type
Thermoelectric	Intensity
Photoelectric	Energy
Thermooptic	
Biochemical	Composition
Physical transformation	Concentration
Chemical transformation	State
Electrochemical	
Spectroscopy	

Implementation of the IC technology for microsystem fabrication represents a very different concept in the sensors technology. Resolutions of $0.001\text{Å}/\text{Hz}^{1/2}$ or sensitivities in the order 10^{-10} N are usual features of such microsensors. The actual achieved precision and the accuracy of MEMS sensors can improve up to one order of magnitude the performances of the classic sensors. The detected input signal can be further fed into the electronic circuitry, conveniently

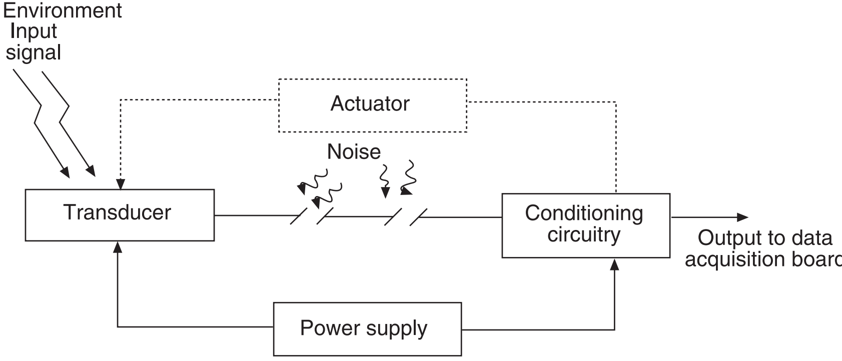

Figure 2 General configuration of a sensor. The dashed line with the feedback actuator shows the configuration of a servo sensor.

located next to the transducer, which modifies the input into a signal which matches the data acquisition system. This is usually equivalent to changing the output to a voltage. The function of the electronic circuitry extends to modifying the sensors' dynamic range to maximize accuracy, filtering the noise, and limiting the measurement spectrum.

Micromachined microactuators are conceived to convert electrostatic, electromagnetic, thermal, or fluid flow energy into mechanical rotation, translation, or oscillation. Although presently the microactuators are created for applications in which the required forces do not exceed μN range, tremendous applications in microbiology have been forecasted. Both linear and rotary microactuators have been built using bulk and surface micromachining technology, although the three-dimensional attributes of the actuators have required special technologies for high-quality vertical pattern fidelity. One main problem of the microactuators relates to the friction and wear of moving parts. The small sized pivots, the complexities associated with total control of clearances between the pivot and the bearing, and the lack of appropriate lubrication methods dramatically reduce the life of the electrostatic motor. However, IC technology has not been modified to accomplish readily assembled devices, such as hinges and articulations. Thus, the alternative technologies permit to compensate for such limitation. Elastic suspensions or levitation principles have been implemented to overcome the friction and wear in rubbing parts. Compliant mechanisms represent another option for MEMS. The compliant mechanisms allow motion through elastic deformations of one or more elements. Motion of compliant segments generally involves large-magnitude nonlinear deflections, which are difficult to predict using the linear beam theory. More accurate prediction of microstructure behavior will require multiphysics nonlinear analyses of the miniature structures. Modeling such devices is thus quite challenging. Application of the surface-micromachined compliant multistable mechanisms on microvalves and microswitches is presently under investigation.

MEMS Materials

Microsystems manufacturing (micromachining) makes use of a large variety of materials. However, only a few are used to build the structural elements. The mechanical properties of these materials are thus of prime interest for the mechanical designer of MEMS. Although the mechanical properties of bulk materials are comprehensively known, the properties of the thin deposited films are strongly dependent on the deposition process and the deposition parameters. **Table 2** provides a list of the most frequently used materials for MEMS structures together with their available relevant properties, as given in the available literature. The physical values range between broad limits, which may be attributed to excessive variations in the measurement methods employed and to the large variance in the properties of the materials. Besides, the thinly deposited films exhibit high internal compressive or tensile stresses, which may to a certain extent influence the mechanical properties of the thin structures. It has been acknowledged that the materials in thin films exhibit higher mechanical strength than the same materials in bulk state.

Apart from the mechanical properties, some materials require other special properties and conditions for the material processing, as they may not withstand subsequent processing. The active materials are specifically used to build the transducer on the measurement element, which is mostly associated with the flexing element in the mechanical microsensors. The deposition and patterning sequences rigorously

Table 2 Mechanical properties of selected materials used in MEMS processing

Material	*Thermal expansion coefficient ($\times 10^{-6}\,°C^{-1}$)*	*Strain limit ($\times 10^{-6}$)*	*Yield strength (MPa)*	*E Young modulus (GPa)*	*Density ($kg\,m^{-3}$)*	*Hardness Knoops (GPa)*	*Poisson ratio*	*Thermal conductivity ($W\,m^{-1} \times °C$)*
Al: film	23	2	0.124	47.2–74	2700–3500	1.3		236
Si: bulk	2.3–4.3	–	7	62–202	2330	5.3–13.1	0.22–0.278	157
Polysilicon: film		3–7	–	120–200			–	
SiO_2: film	0.41–31.9	112	8.4	46–95	2200	8.2–18	0.17	1.10–1.7
Si_3N_4: film	0.8–3.9	37	1.4	100–380	3200	34.8	0.22–0.27	9.2–30
SiC: film	4.7–5.8	–	21	302–450	3200	24.8–29.6	0.183–0.192	20.8–120
PVDF: film	6–250	–	–	2	1780			
Polymide: film	3–140	–	–	7.5–15			0.1–0.45	
Pt: film	8.9–10.2	1	–	170	21 440			73
Monosilicate glass t059: film		–	–	40–60	2250	5–7		
Diamond-like carbon (DLC)		–	–	150–800				
Au: gold	14.1–16.5	–	–	80	19 280			315

require certain standing limits for the deposited material. One should bear in mind that the same materials are used to build the IC, and thus, material selection must avoid any incompatibility problems that could jeopardize the IC performances due to the fabrication.

MEMS Fabrication Technology

MEMS fabrication mostly makes use of established IC processes. Apart from the rigid processing sequence, some new techniques have been developed and implemented to substitute for the lack of flexibility of the standard IC. They appropriately use the unconventional machining together with the standard machining processes. Thus, LIGA (deep-etch lithography, electroforming, and plastic molding), laser-assisted chemical vapor deposition (CVD), electroplating, chemical plating, and even conventional machining form the most common manufacturing techniques.

In lay terms, accomplishment of MEMS through surface micromachining is done through deposition of specific thin films (required by the IC process), patterning and etchings of the deposited material on undesired areas, followed by other successive depositions, patternings, and etchings arranged in stacks. The desired structure is thus fully completed and embedded into the consecutive layers of depositions. Postprocessing is performed to remove the sacrificial films and release the free-standing structure.

Table 3 schematically illustrates the core of the IC-for-MEMS fabrication processes. The table presents the three main processes: deposition, patterning, and the removal of sacrificial layers. These processes are subject to considerable variations in the process parameters depending upon the technology implemented. The deposition techniques have reached performance levels that enable the deposition of films with adequate mechanical and electrical properties.

Further, **Table 4** gives a list of most other common processes used to realize MEMS. As can be seen, standard machining processes are included in the list, since hybrid accomplishment of MEMS through IC and standard processes is an alternative that is still under appraisal. Some of the standard machining processes are most instrumental for packaging. Most of the standard machining processes, however, require individual manipulation of parts, which represents a bottleneck for a batch fabrication stream.

The etching process marks the postprocessing of the microstructure. Release of the free-standing structure represents a challenge, since the electronic circuitry, the contact pads, and the structure itself have to withstand the etching. The costs associated with postprocessing and packaging of MEMS often contribute to a significant increase in the cost of the MEMS. The low-cost postprocessing techniques, invariably performed outside the silicon foundry, are thus extremely desirable.

The selectivity of the etchant with respect to the passivation and structural films is of most interest in surface micromachining. **Table 5** presents the most popular etching recipes for Si, glass, Si_3N_4, Al, and Au along with the corresponding etch rates.

Table 3 Description of fabrication processes for MEMS

Process	*Type and method*	*Sketch*
Thin film deposition		
Uniform deposition of selected materials on the entire surface of the wafer	Chemical vapor deposition (CVD)	
	Physical vapor deposition (sputtering, vaporization)	
Lithography		
Batch printing on substrate 2-D and 3-D features on photo-sensitive polymer	UV photolithography	

Table 3 Continued

Process	*Type and method*	*Sketch*
	E-beam lithography	Photoresist spin coating; Pre-baking; If the photoresist thickness is ≈ 300 μm; Substrate; e-beam gun; Development; Post baking
Etching	Deep etching (crystallographic)	trench; mask; 54.74°; Si; Hole
Selective removal of undecided material from designated areas exposed to the etchant	Anisotropic – (100) silicon wafer	
	Isotropic: Si wafer	Mask; Cavity; Si
	Thin film etching	Structural layer; Sacrificial; Substrate
	Sacrificial: any material etching	

Table 4 Alternate processes used in MEMS manufacturing

Process	*Alternatives and issues*
Electroforming	Electrochemical deposition (plating): contamination
	Anodizing: contamination
	Polishing: not very productive
Surface processing	Ion implantation
	Diffusion: high temperatures
	Annealing: high temperatures
Coating	Dipping: all sides are covered
	Spinning: high process variability
	Spraying: uniformity issues
	Serigraphy: alignment
Forming	Hydro: contamination, accuracy
	Drawing: high temperature or high built-in stress
Extrusion	Direct/indirect: accuracy
Molding	High-pressure injection
	Vacuum: accuracy
	Dipping: filling
	Compression
Machining	Turning: fixture
	Milling: high forces
	Drilling: chip removal
	Sawing
	Electrochemical discharge
Finishing machining	Grinding: high forces
	Polishing: low efficiency
	Lapping: low efficiency
Microcutting	Laser: low efficiency
	Electron beam
	Electrochemical discharge: contamination, minimum size
Joining	Riveting: size (microsize riveting under investigation)
	Screwing: size
	Soldering: strength
	Brazing: high temperature
	Elastic
Bonding	Anodic: high temperature and voltage
	Thermal: high temperature
	Adhesives: limited life
Welding	Laser
	Electron beam
	Electric spot: size
	Electrochemical
Wire bonding	Ultrasonic
	Thermal: high temperature

The selectivity of the anisotropic etchant versus certain crystallographic planes is responsible for the sculpturing into silicon of V or U trenches that are conveniently used to create bulk micromachined structures. **Table 6** presents the most used silicon anisotropic etchants, typical etching temperature, etch rate, and selectivity.

The essential electrochemical etch reactions involve oxidation–reduction and dissolution of the oxidation products by complex etching agents. Both electrons and hole carriers exist at the silicon surface. Oxidation of silicon atoms takes place at the anodic sites, while the oxidant is reduced at the cathodic sites. The etching mechanism can be summarized as follows:

- Injection of holes into the semiconductor $Si + 2\oplus^{+} \rightarrow Si^{2}$
- Attachment of hydroxyl group OH^{-} to Si^{2+}, e.g. $Si^{2+} + 2(OH^{-}) \rightarrow Si(OH)_2$
- The dissociation of water $H_2O \leftrightarrow OH^{-} + H^{+}$
- Reaction of the hydrated Si with complexing agent in the solution
- Dissolution of the reacted product into etchant solution

These etching mechanisms, however, do not fully describe the crystallographic anisotropic etching of silicon, and the temperature and stress dependences or the selectivity.

More accurate etching can be carried out in reactive gases. The anisotropic etching of silicon in gas is no longer driven by the crystallographic structure. Thus, the etchant no longer follows the crystallographic direction (111), like the wet anisotropic etchants, but the cut strictly follows a perpendicular direction to the masked surface. **Figure 3** illustrates isotropic and anisotropic etching. **Table 7** gives the gas etchants for materials most commonly used in MEMS fabrication, together with specific etch rate and selectivity versus various masking materials.

MEMS Packaging

The basic considerations for MEMS packaging are:

- Connections to the chip for signal and power leads
- Means of cooling of the chip if necessary
- Mechanical structure to support and protect the chip
- Controlled-pressure environment to reduce the viscous damping of the flexing structure and provide access for the measurand to the sensing area

Satisfying all the requirements for a robust package has proven to be a very difficult task. The selected materials must possess compatible thermal coefficients of expansion, or the structure must comprise the means to release the resulting mechanical stress, and excess of heat.

Temperature changes may arise either from the chip operation or changes in the operating environment. The connections and the package should enable low noise transmission and a high-fidelity path for signals to and from the chip, and robustness of connections. Applications with specific considerations include, but are not limited to, operations in hostile environments, hybrid multichip packages,

Table 5 Wet etching solutions and etch rates for MEMS materials

Material	*Etchant solution*	*Etch rate*
Polysilicon	6 ml HF, 100 ml HNO_3, 40 ml H_2O	800 nm min^{-1}, smooth edges
	1 ml HF, 26 ml HNO_3, 33 ml CH_3COOH	150 nm min^{-1}
SiO_2	Buffered HF (BHF) (28 ml HF, 170 ml H_2O, 113 g NH_4F)	100–250 nm min^{-1} at 25°C
	1 ml BHF, 7 ml H_2O	80 nm min^{-1}
Borosilicate glass (BSG)	1 ml HF, 100 ml HNO_3, 100 ml H_2O	30 nm min^{-1} for 9 mol% B_2O_3, 5 nm min^{-1} for SiO_2
	4.4 ml HF, 100 ml HNO_3, 100 ml H_2O	75 nm min^{-1} for 9 mol% B_2O_3, 13.5 nm min^{-1} for SiO_2
Phosphosilicate glass (PSG)	Buffered HF (BHF)	550 nm min^{-1} for 8 mol% P_2O_5
	1 ml BHF, 7 ml H_2O	80 nm min^{-1}
Si_3N_4	HF	14 nm min^{-1}, CVD at 1100°C
		75 nm min^{-1}, CVD at 900°C
		100 nm min^{-1}, CVD at 800°C
	BHF	0.5–10 nm min^{-1}
	H_3PO_4	10 nm min^{-1} at 180°C
Al	4 ml H_3PO_4, 1 ml HNO_3, 4 ml CH_3COOH, 1 ml H_2O	35 nm min^{-1}, high resolution
	16–19 ml H_3PO_4, 1 ml HNO_3, 0–4 ml H_2O	150–240 nm min^{-1}, coarse
	0.1 mol $K_2Br_4O_7$, 0.51 mol KOH, 0.6 mol $K_3Fe(CN)_6$	1 μm min^{-1}, coarse
Au	3 ml HCl, 1 ml HNO_3: aqua regia	25–50 μm min^{-1}
	4 g KI, 1 g I_2, 40 ml H_2O	0.5–1 μm min^{-1}, resist mask

Table 6 Moncrystalline silicon etchants, etching rates and selectivity

Etchant	*Typical composition*	*Temperature (°C)*	*Etch rate (μm min^{-1})*	*Anisotropy (100)/(111) etch rate ratio*	*Dopant dependence*	*Masking films (etch rate of mask)*
Ethylene diamine pyrocatechol (EDP) in water	750 ml 120 g 100 ml	115	0.75	35:1	7×10^{19} cm^{-3} boron reduces etch rate by about 50	SiO_2 (0.2 nm min^{-1}) Si_3N_4 (0.01 nm min^{-1})
	750 ml 120 g 240 ml	115	1.25	35:1		
KOH in water	44 g 100 ml	85	1.4	400:1	10^{20} cm^{-3} boron reduces etch rate by about 20	Si_3N_4, SiO_2 (1.4 nm min^{-1})
KOH in isopropyl alcohol	50 g 100 ml	50	1.0	400:1		
Tetramethyl ammonium hydroxide in water (TMAH)	25 g 75 ml	85	0.6	200:1	$\geq 2 \times 10^{20}$ cm^{-3} boron reduces etch rate about 25 times	Si:SiO_2 (1000:1)
	15 g 85 ml	85	0.5	200:1		
Isotropic etchant HF HNO_3 CH_3COOH	10 ml 80 ml 30 ml	22	0.7–3		Reduce rate by 150 for phosphorous and boron 10^{17}·cm^{-3}	SiO_2 (30 nm min^{-1})
	25 ml 50 ml 25 ml	22	4			Si_3N_4 SiO_2 (70 nm min^{-1})

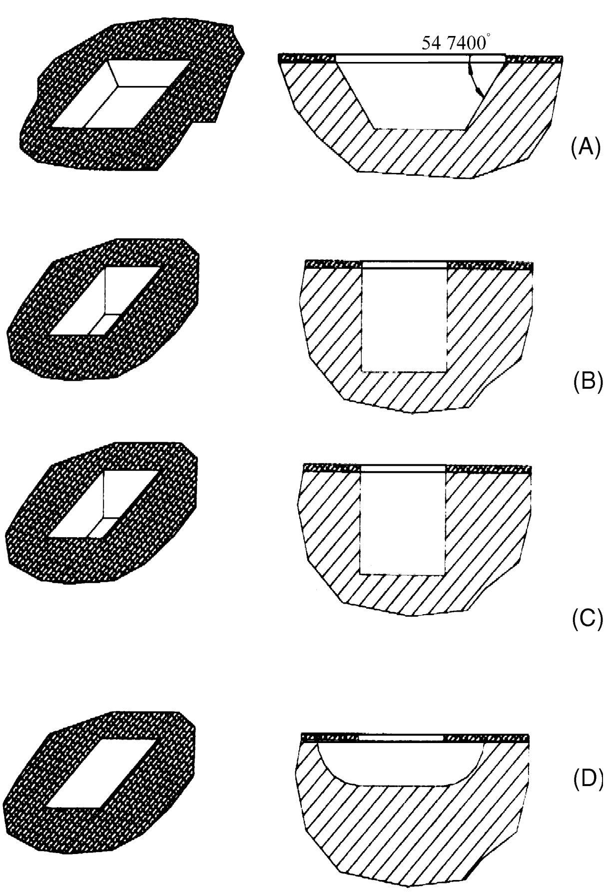

Figure 3 Section through anisotropic and isotropic etched silicon features. (A) Wet etching of (100) Si orientation; (B) wet etching of (110) Si orientation; (C) dry isotropic etching of Si; (D) isotropic etching of Si in XeF_2.

vibration control, and direct exposure of portions of the chip to outside stimuli (i.e., light, gas, pressure, and temperature).

MEMS Design

The observations on the dynamic behavior of MEMS indicate that they do not follow the pattern of similar geometric macrostructures. The design of MEMS requires a perfect knowledge of the capabilities and drawbacks of the manufacturing processes. Both bulk and surface micromachining impose specific constraints on the design that are often reflected in the geometry of the features. Both bulk and surface MEMS could be better designed using a computer-aided design (CAD) tool which are built to include the constraints of the manufacturing process. The layout design level is usually carried out on IC-compatible design tools, which enable the design of the electronic circuitry. Simulations of the dynamics of both electronic circuitry and the mechanical structure modeled as an electronic circuit help to improve the performance of the coupled electromechanical system. The simulation uses models which are created based on analogous electrical circuit elements. A comparison of the mechanical, fluid, and thermal elements with the electrical element is given in **Table 8**. It is important to note that other first-order analogs are accepted and used in simulations. The selection of analogs, however, may depend on the likeness of current and voltage used in describing the mechanical physical quantities.

Table 7 The gas etchants for materials used in MEMS, etch rate, and selectivity versus Si, SiO_2, and photoresist

Material	*Etching gas*	*Etch rate (nm min^{-1})*	*Selectivity*		
			vs silicon	*vs SiO_2*	*vs photoresist*
Si	$SF_6 + Cl_2$	100–450		80	5
Polysilicon	Cl_2	50–80		30	5
SiO_2	$CF_4 + H_2$	50	20		5
PSG	$CF_4 + H_2$	80	32		8
Al	$BCl_3 + Cl_2$	50	4	22	7

Table 8 Comparison of physical elements

	Dissipative	*Current storage*	*Potential storage*
Electric	Resistance	Inductance	Capacitance
Mechanical	Damper	Spring	Mass
Fluid	Fluid resistance	Fluid inertance	Fluid capacitance
Thermal	Thermal resistance	–	Thermal capacitance

Next Page

One of the challenges a designer has to face in modeling is to establish the figure number of the squeeze damping and the elastic constant for the continuum beam or plate element. Attempts to express analytically the equivalent stiffness of cantilever and double-supported micromachined beams have been done, but the simple analytical expressions do not always match the experimental available data. More accurate solutions are accomplished when the finite element analysis (FEA) is used in conjunction with the appropriate material data. Nonlinear characteristics of the material or nonlinear behavior of the structure can be simulated through appropriate description of the material and elements. Sufficient accuracy can be achieved by conveniently refining the mesh. A parametric design used in conjunction with multiple variable optimization algorithms can enhance the performance of the structures. Stress–strain, modal, dynamic, thermal, electromagnetic or CFD analyses can be run once a suitable model has been conceived. The output can provide essential information that may lead to improved performance of the microstructure. Some commercial codes can perform multivariable optimization, which would ease the task of the designer.

However, an overall strategy of the entire manufacturing flow, including packaging, must be planned before the analysis is carried out. Important pieces of information such as damping of the structure reside in the environment in which the structure will work and the operating temperature. Thus, the dynamic properties will strongly be influenced by the surrounding gas/fluid in which the flexing structure performs. Before the layout design is finalized, simulations of selected deposition and etching processes may be run to insure that critical features will be accomplished within the permitted tolerances.

Figure 4 illustrates the graphic output of a stress analysis performed on the section of a plate subjected to uniform pressure loading. Appropriate meshing yields the stress distribution across the thickness of the plate, which can further be used by the designer to establish the most appropriate location of the piezoresistive gauges.

After prototyping, manufacturing, and testing, the models are adjusted based on the empirical data obtained from measurements. Presently, the integrated modeling of MEMS is still in its infancy, although efforts have been made to understand and model the individual manufacturing processes, such as etching, crystal growth and physical deposition. Although not explicitly stated, it is apparent that analytical models of microstructures are also used and continuously improved, as test data become available. Modeling of electromechanical–fluid–thermal systems is thus of much interest to the designer. One of the main needs at this time is to build a good microscale data bank of parameters and material properties that can be used in the modeling and design of microsystems.

Miniaturization of mechanical systems establishes a unique momentum in both classic and emerging technologies. MEMS enables a new approach in making, running, and controlling systems and processes. Micromechanical devices and systems are essentially smaller, lighter, faster, more precise, and

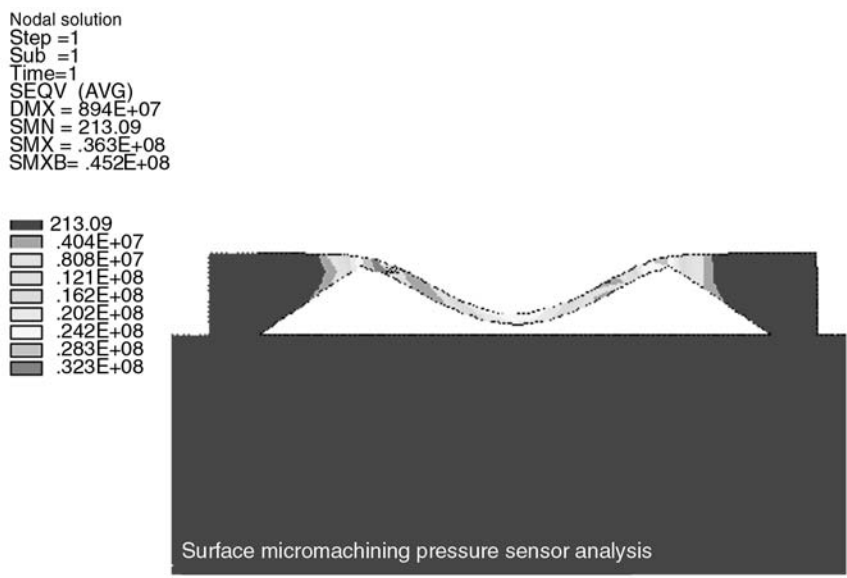

Figure 4 (see Plate 42). The output graphic file of an analysis of a silicon plate subjected to uniform distributed pressure loading.